FINITE ELEMENT ANALYSIS OF A COMPOSITE CYLINDRICAL SHELL WITH A CUTOUT UNDER FATIGUE LOADING

THESIS

Joshua T. Boatwright, Captain, USAF

AFIT/GAE/ENY/00M-03

DEPARTMENT OF THE AIR FORCE

AIR UNIVERSITY

AIR FORCE INSTITUTE OF TECHNOLOGY

Wright-Patterson Air Force Base, Ohio

20000803 145

The views expressed in this thesis are those of the author and do not reflect the official policy or position of the Department of Defense or the United States Government.

FINITE ELEMENT ANALYSIS OF A COMPOSITE

CYLINDRICAL SHELL

WITH A CUTOUT UNDER FATIGUE LOADING

THESIS

Presented to the Faculty of the School of Engineering and Management

of the Air Force Institute of Technology

Air University

In Partial Fulfillment of the

Requirements for the Degree of

Master of Science in Aeronautical Engineering

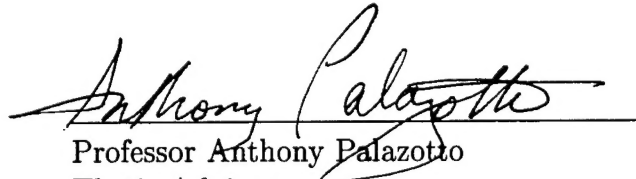Joshua T. Boatwright, B.S.
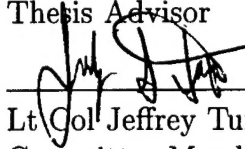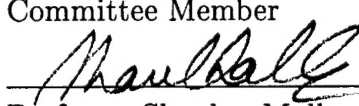
Captain, USAF

March, 2000

FINITE ELEMENT ANALYSIS OF A COMPOSITE

CYLINDRICAL SHELL

WITH A CUTOUT UNDER FATIGUE LOADING

Joshua T. Boatwright, B.S.

Captain, USAF

Approved:

Professor Anthony Palazotto   Date 3/6/00
Thesis Advisor

Lt Col Jeffrey Turcotte   Date 03 MAR 2000
Committee Member

Professor Shankar Mall   Date 3/9/00
Committee Member

Acknowledgements

I would first like to thank Dr. Palazotto for his optimism, guidance, understanding, and support. Thank you for taking half an idea and making it a reality. You are a giant among men and I will miss our Tuesday meetings. I would also like to thank Dr. Steven Walker of the Air Force Office of Scientific Research for sponsoring this research.

Further thanks is required for Dr. Sam Naboulsi. First of all, thank you for taking time away from your upper-echelon research to provide help. Your knowledge and experience in finite element analysis were the key to unlocking the myriad of problems I could not solve. Good luck in the future, go Dawgs, and you can have the "zoo's" computers back now.

My wife, Kammie, is due a bushel of thanks for her unwavering support and love. Thank you for being so understanding and supportive. Finally, all credit goes to God, for He alone is worthy.

<div align="right">

Joshua T. Boatwright

</div>

Table of Contents

List of Figures

vii

List of Tables

AFIT/GA/ENY/00M-03

Abstract

A higher-order shell theory is used to analyze compressive and tensile loads on a graphite/epoxy laminated cylinder containing a square cutout. The Hashin failure criterion is used to determine failure in the fiber, matrix, or lamination. Once failure occurs, the appropriate stiffness terms are reduced. This failure causes a redistribution of stress, leading to further failure. In order to account for the loss of residual strength due to cyclic loading, the stiffness matrix is further reduced at each new increment of load or displacement. The objective is not to determine the S-N curve for the material, but rather to determine the damage, displacement, and stress distribution in a complex configuration under fatigue loading using a progressive failure and stiffness reduction approach. The failure progression for static loads is determined and used as an indicator for the cyclic loads. It is shown that as the stiffness decreases, the global displacements increase, resulting in more failure until the entire panel fails.

FINITE ELEMENT ANALYSIS OF A COMPOSITE CYLINDRICAL SHELL WITH A CUTOUT UNDER FATIGUE LOADING

I. Introduction

1.1 Motivation

A common problem among pressurized cylinders, such as aircraft fuselages, are fatigue cracks initiating from cutouts. These cutouts are often rectangular in shape, such as doors and windows in a fuselage, resulting in large stress concentrations at the corners. A better understanding of the stress and damage due to the presence of cutouts will hopefully lead to improvements in composite structural design, and this research specifically targets cylindrical shells due to their common structural applications.

Fiber-matrix composite materials are being increasingly used in structural applications, including ones involving the above-mentioned geometry. Their tailorable properties result in a high strength-to-weight ratio, which is a performance-driver in many applications. They do not often behave as homogeneous materials do, requiring new techniques and research. For reference, the term "composite" in this thesis is meant to describe fiber-matrix laminates, where parallel continuous fibers are surrounded by a matrix. This defines a unidirectional laminae, and these may be stacked in different fiber orientations to develop a multidirectional laminate. Unless

otherwise mentioned, the matrix is assumed to be constructed of resin or epoxy and not metal.

One of the first steps in design is to account for the static loading. Many components, however, fail in fatigue rather than static loading. Techniques to analyze fatigue for isotropic materials are not always applicable to composite materials, and new methods must be explored.

1.2 Background

1.2.1 Shells.
Classical plate theory falls short in capturing the state of stress and strain in a curved shell, requiring the development of shell theory. Shell theory attempts to simplify this analysis by modeling thin structures as two-dimensional problems. This is done by assuming the in-plane loads are dominant, which allows the use of a datum surface to characterize out-of-plane loads. In this way, the three-dimensional problem is represented two-dimensionally. Because of the complicated nature of curved shells, several different theories have been proposed.

One of the first shell theories was the Love (1) theory, which applied Kirchhoff type assumptions to a shell. This is a classical linear approach. Donnell (2) applied the generalized Kirchhoff-Love shell theory to thin cylindrical shells. A more detailed shell theory uses Reissner (3) and Mindlin (4) (RM) assumptions, which relaxes the restriction that plane sections remain normal to the midplane. A nonlinear shell theory, the Simplified Large Rotation (SLR) theory, was developed by Palazotto and Dennis (5). This theory has been validated and used for a variety of loading conditions, and is the theory used in this research. The power of this theory is the ability to account for the geometric nonlinearities that occur, especially for a thick shell or for instability such as buckling. It has improvements over both the Donnell and RM theories, as will be described in Chapter 2.

Hatfield (6) used the SLR theory and Finite Element Methods (FEM) to analyze composite cylindrical shells with a large, rectangular cutout under compression loading. Various configurations were chosen and compared against experimental results. Both quasi-isotropic and cross-ply lay-ups were studied, in thicknesses ranging from 8 plies [1.04 mm (0.041 in)] to 24 plies [3.13 mm (0.123 in)]. Quasi-isotropic refers to combinations of $0°, 90°$, and $\pm 45°$ laminates, to account for longitudinal, transverse, and shear loads (hence, responding similar to an isotropic material). Cross-ply refers to a layup containing $0°$ and $90°$ oriented plies. This work studied the geometric nonlinearities present during large displacements and moderately large rotations—such as during collapse—as well as the effects of transverse shear in thick shells.

1.2.2 Cutouts.

Senocak and Waas (7) pursued optimum reinforcement for a laminated cylindrical shell with a cutout. Collapse due to a static buckling load was determined using the Donnell shell theory. Then a stress function was assumed and applied to the Donnell equations. This resulted in an expression for the forces, bending, and twisting moments if a cutout were present. Once this expression is known, the forces and moments required to resist bending can be determined. From this information, a reinforcement is designed to increase the shell's collapse load.

Hilburger, Waas, and Starnes (8) studied the interaction between bending and membrane reactions due to the presence of a cutout in a cylindrical shell under a static compression and internal pressure load. The nonlinear code STAGS was used in the analysis, and it was determined the cutout introduces local buckling which, reduces the overall collapse load of the cylinder.

Kapania, Haryadi, and Haftka (9) used an alternating global/local analytical approach to determine the stress field around circular and elliptical holes in flat composite plates. First, a global, numerical solution is obtained using the Ritz method

with an assumed displacement function. These resulting displacement and slope boundary conditions are then applied to a local finite element model to determine the stress field around the cutout. For a circular hole, the local analysis proved to be extraneous, while for elliptical holes, the extra local analysis increased the accuracy of results.

Rhee, He, and Rowlands (10) take a similar approach to determining the stress around a cutout in a composite. First, a finite element analysis is performed on a plate without a cutout, where a single element encompasses the area normally occupied by the cutout. The displacement boundary conditions for this element are then applied to a Gerhardt hybrid element (11). This hybrid element contains a cutout, which must be described by a mapping function. The displacement around the cutout are determined from the boundary conditions and the cutout geometry, which can be related to photomechanical fields such as Moiré's. This information can then be used to determine the stress.

Numerical stress distributions for a thick (nonlinear) curved shell with circular or elliptical cutouts was developed by Chao, Diankui, Xingrui, and Benli (12). The complex variable method and conformal mapping are used to study stress concentrations in thick shells. The complex stress function converts the shell's governing equations into three Helmholtz's equations. The stress function is represented as an infinite series.

1.2.3 Failure Criteria.

Another approach to analyzing composite materials is through the use of failure criteria. In general, a failure criterion compares load parameters, such as the current state of stress, with the material's determined parameters, such as ultimate strength values. If the criterion exceeds this value, failure is determined to occur. One of the early developers of a failure criterion for composites was Tsai (13). His work was incorporated with other theories to develop such criteria as Tsai-Hill (14) and Tsai-Wu (15). The problem with the

Tsai-Hill criterion is its inability to account for differing failure strengths in tension and compression (16). Hoffman (17) corrected this problem by adding a quadratic expression. Tsai-Wu used a general quadratic expression to add robustness, but this resulted in a cross-ply material characteristic which is not easily determined (16). Hashin (16) developed a simple but powerful criterion tailored to composite materials. It can handle differing strengths, and determines whether failure is due to tension, compression, or shear in either the fiber, matrix, or by delamination between layers. This is the criteria used for the present research and will be discussed in more detail later.

Lee (18) incorporates failure criteria with finite element analysis to 1) determine the stress distribution 2) identify damage and failure modes and 3) compile damage accumulation to determine ultimate strength. The failure criterion developed by Lee is similar to Hashin's, however, it does not incorporate as many terms. Lee identifies procedures for a progressive failure approach in a finite element analysis. First, the finite element analysis is performed and the stress distribution determined. Once the stress is known, the failure criterion is applied. If damage has occurred, the appropriate stiffness terms are reduced. The externally applied stress is then increased and the process repeated. This continues until failure of the entire panel occurs. This approach is used as the basis in this research. It is important to note that Lee admits no delamination occurred during his analysis, which does not seem to match experimental results.

Falzon, Steven, and Xie (19) used the Tsai-Hill failure criterion to optimize cutouts in composites. They performed a finite element analysis where elements were eliminated in the regions in which the highest failure occurred. This allowed a broader redistribution of stress, until the cutout shape was optimized. As expected, for an equal cross-ply load, the optimal cutout is a circle. For a pure shear load, the optimal cutout is square rotated 45 degrees from the panel edges. Under combined

cross-ply and shear loads, an elliptical shape is optimal. The basis for the present research explores geometries which are not allowed to be optimal.

Spottswood (20) used failure criterion in a progressive damage model to determine failure in a cylindrical shell under a transverse load. Three failure criteria, the maximum stress criterion, Lee's criterion, and Hashin's criterion were used in comparison.

1.2.4 *Fatigue.*

A fatigue load is a load where the applied magnitude is below the failure threshold but is applied over many cycles. This cyclic load causes micromechanical damage to the structure (21). This minute damage causes local stress concentrations, which locally increase the damage zone. Finally, over time, this micro-damage coalesces into larger, macro-damage. Once the macro-damage is present, stress concentrations occur over much larger regions. This causes the macro-damage to grow and expand to an increasingly larger region, until finally, the structure can no longer carry the static load.

The configuration or geometry of a structure also affects its fatigue life. Both research and experience have shown that notches, holes, and cutouts cause a local increase in the stress distribution (21). Research has also shown that sharper notches and corners cause a larger local stress concentration than more rounded, smooth cutouts (21). This is comparable to thinking of stress as water flow and the structure as an aquaduct. A sharp reduction in the aquaduct size requires the water to increase its velocity almost instantaneously, resulting in a large disruption of water flow in the region of reduction, while a gradual, smooth reduction allows the water to accelerate smoothly, over a longer distance. Likewise, sharp cutouts cause a disruption of stress, resulting in a large stress concentration. Obviously, then, it is favorable to eliminate cutouts or design them as non-interfering as possible, such as the work by Falzon, et al. mentioned above. This is often difficult in applied structures, however, for reasons such as geometry limitations or manufacturing difficulty.

Tools have been developed to predict the time until a material fails in fatigue, or its *fatigue life* (21). On the micro-level, the field of fracture mechanics attempts to define the stress concentrations around geometry such as notches, holes, and crack tips. On the macro-level, most isotropic materials and several composite laminate materials have fatigue life or S-N curves. The fatigue stress is usually denoted S while the number of cycles to failure is N. However, most damage initiates on the micro-level at some inherent defect which is impossible to predict. Also, the number of other inherent defects within the material affect how fast the damage changes to the macro-level. Therefore, predicting fatigue life—either through experimental or computational means—is not an exact science.

1.2.5 *Fatigue in Composites.*

Fracture mechanics and other fatigue analysis techniques were initially developed for isotropic materials (21). For an isotropic material, loading results in a single crack that grows until the structure can no longer carry the applied load. A composite laminae, made up of fibers and a matrix, are stacked into a laminate. There are many failure modes for a composite material, and they may develop independently or as a result of other types of failure (22). There are also several mechanisms to resist failure growth. If the matrix cracks, crack growth is resisted by the continuous fiber. If a fiber fails, the matrix can distribute the failed fiber's load to other fibers. If a ply disbonds, each layer is still able to carry in-plane loads. Therefore, the initiation and interaction of these damage modes must be considered for composite laminate fatigue.

Agarwal and Broutman (22) identify the various levels of fatigue damage as it occurs in multidirectional composites. The first effect is the debonding of the fiber and matrix in the most transverse plies. For example, the plies oriented 90° to the load (and hence the most transverse) would develop these disbonds first. This develops into a crack which extends vertically to the top and bottom of the ply. These cracks arrest at plies with fiber orientations parallel to the load (or the principal direction). These cracks occur at several locations within the transverse

plies, until they saturate. This has been termed the *characteristic damage state* or CDS by Reifsnider, Henneke, and Stinchcomb (23). The crack tips, however, cause a local stress concentration at the interface between plies, which cause delamination. This delamination grows until large stresses develop in the principal direction plies, causing matrix cracking and fiber debonding. Also, the plies are separated and become independent, further increasing local stress until fiber breakage occurs. Large scale fiber-breakage occurs near 90% of the composite's fatigue life (22).

Fatigue of composite materials was also studied by Talreja (24). He proposed that fatigue of composites be characterized by strain instead of stress, since the state of stress within a composite can vary depending on ply layup. He identifies three important regions in the fatigue life of a unidirectional composite. The first is the endurance limit, which may be defined as the value of strain below which fatigue failure does not occur. Typically, this is the strain below which matrix cracking does not occur, denoted as ϵ_m. The upper region is the strain where fiber breakage occurs, or ϵ_c. For all practical purposes, this is the same as static failure, and fatigue life is minimal. In the middle is the region of fatigue, where matrix cracks initiate. This damage leads to further cracks and delaminations, which are the damage growth mechanisms leading to fatigue failure. For a multidirectional laminate, a different lower bound may occur. For laminae in directions transverse to the load, disbonding between the fiber and the matrix may be present. This is extreme at the 90° orientation, and lessens for decreasing fiber orientation angles. This research correlates well with the failure progression described by Agarwal and Broutman, above.

One of the fracture mechanics techniques applied to composites is through determining the strain energy release rate, G. This method has been used by Ericson, et. al. (25) as well as Jen and Sun (26). Another method is a strength based approach. In this approach, an expression for the residual strength of the composite

is developed as a function of the number of cycles. According to Sendeckyj, three key assumptions determine this approach (27):

1. A Weibull distribution describes the static strength.

2. The residual strength after n cycles is related to the initial static strength through a deterministic equation, based on the S-N curve.

3. Failure occurs when the residual strength—the remaining material strength of the structure–reduces to the value of the applied stress.

This method has been explored more recently by Reifsnider (28), as well as Schaff and Davidson (29).

Stinchcomb and Bakis (30), reflecting on the work of Jamison and Reifsnider (31), note that the stiffness of a graphite epoxy laminate reduces over the fatigue life of a composite. An equation can be used to account for this stiffness reduction over time. This technique is explained by Sendeckyj (27). Poursartip, Ashby, and Beaumont (32) used this technique to study delamination under fatigue loading, and their research is based on the work of O'Brien (33). O'Brien used a rule of mixtures to account for the loss of stiffness due to delamination.

Jen, Kao, and Hsu (34) also studied the onset of delamination by analyzing stiffness reduction. They used a mathematical model for the stress distribution, and applied the resulting stress to a failure criteria. Once the criteria was exceeded, it was determined that delamination occurred. They were unable, however, to determine the resulting stress redistribution due to the delamination.

Barboni, Carbonaro, and Gaudenzi (35) also studied the onset of delamination due to fatigue. Using a Multi-layer Higher-Order Laminate Theory which takes a two dimensional approach to a three dimensional problem, they characterize the out-of-plane stress which develops near a free edge. An interlaminar failure criterion is used to determine when and where the onset of delamination occurs. Their theoretical work, however, only focused on the onset of delamination. Experimentation was

also performed, and they concluded delamination is not critical for [0/90] layups, in static or fatigue loading. For [+45/ − 45] layups, delamination initiates in the static case near the panel failure value. But for fatigue, delamination can be a driver in the reduction of fatigue life for this layup.

Another approach is to incorporate fatigue parameters into the failure criteria. This approach has been taken by Hashin and Rotem (36), Fawaz and Ellyin (37), and most recently, Philippidis and Vassilopoulos (38). These criteria are similar to quasi-static failure criteria, except they contain factors that are functions of fatigue data. This data is normally acquired through the determination of an S-N curve. The downside to this approach is the reliance on experimental data. The amount of required data can be extensive for different configurations and loading conditions.

Work by Tahiri, Hénaff-Gardin, and Lafarie-Frenot (39) shows some interesting relationships between static and fatigue damage development and stiffness reduction. Their research involved T300/914 graphite epoxy, $[+45_2/ − 45_2]_{2s}$, specimens. Under cyclic tests, they show a steady increase in the number of cracks, while for quasi-static loading, cracks do not develop until the load is very high. Stiffness reduction, however, has the inverse relationship. The material stiffness degrades a large value in quasi-static loading (up to 75%), but only varies slightly in fatigue loading (around 10%).

As seen from this literary review, cutouts and fatigue in composites are all being actively studied, with many different approaches being taken. Further research is warranted in these areas to better define the affects on composite structures.

1.3   Objective

The objective of this research is to develop a technique to characterize the displacement, stress, and subsequent failure that occurs in a cylindrical composite shell with a square cutout under a fatigue load. This research involves a complex combi-

nation of geometry, materials, and loading. Due to recent advances in both theory and computing power, it is now possible to analyze such complicated combinations.

1.4 Approach

The approach of this research is to use a Finite Element Model (FEM) to determine the stress distribution in a cylindrical shell with a large rectangular cutout. First, a static analysis is performed to determine the shell ultimate load. Then, a fatigue load is applied at a percentage of the ultimate load. This is done for tension as well as compression.

The finite element code was developed by Dennis and Palazotto and uses the SLR theory (5). FEM methods provide the stress, strain, and displacement for virtually any location at any ply in the cylinder. This provides a detailed description of the stress, not only within the element, but on a ply-by-ply basis as well. This is a benefit over current experimental analysis techniques such as strain-gages, photoelasticity, Moiré diffraction, and Stress Pattern Analysis by measurement of Thermal Emission (SPATE), which have a limited ability to combine stress intensities and distributions at any location.

Failure criteria and stiffness reduction techniques are incorporated to account for damage. The Hashin failure criterion is chosen for its detailed stress expressions and its ability to distinguish between matrix, fiber, and delamination failures in either tension or compression. Once failure is determined to occur by the failure criterion, the appropriate elemental stiffness terms are reduced according to the type of damage. The stiffness terms are also arbitrarily reduced each loading cycle to represent the effects of fatigue on a composite. Therefore, this is more of a damage accumulation/stiffness reduction approach to fatigue versus the traditional fracture mechanics approach.

II. Theory

It is important to discuss the theory behind the techniques used in this research. The basis of the analysis is the SLR shell theory, which allows use of more complicated geometries than just a flat plate. It is also necessary to discuss the finite element techniques used to implement the theory. The basis for the development of the Hashin criteria is described. Finally, stiffness reduction is presented as a technique for analyzing composite materials undergoing cyclic loading.

2.1   Simplified Large Rotation Theory

As mentioned before, the SLR shell theory is used for two reasons: 1) it allows 2-D analysis of a 3-D problem 2) it accurately handles geometric nonlinearities from the response of a curved panel. The SLR theory is fully explained in (5). For completeness, many of the important aspects of the theory will be discussed here.

2.1.1   Assumptions.   One of the main differences between the numerous shell theories is the assumptions used. The main assumptions used in the SLR theory are as follows: 1) The shell thickness is small compared to the in-plane dimensions. 2) The shell response is characterized based on its original, undeformed configuration. This is known as a "Lagrangian" approach. Therefore, the internal strain energy is characterized by Green's strain tensor and the Second Piola-Kirchoff stress tensor. 3) The material response is assumed to be linear, while geometric nonlinearities are allowed to occur. A geometric nonlinearity results from large displacements and moderately large rotations. 4) Because the shell is thin, stress in the out-of-plane, or σ_3, direction is zero. 5) The through-the-thickness, or transverse, shearing strains are zero on the top and bottom surfaces but are parabolic between the two. Therefore, the transverse stresses also have this representation. 6) While the stresses and strains are developed in the Lagrangian coordinate system,
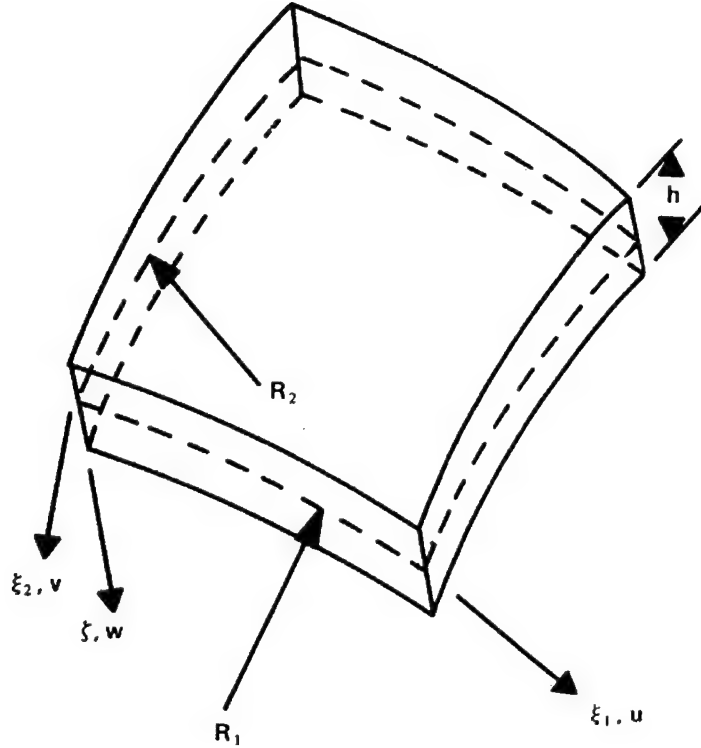
Figure 2.1   Shell Reference Geometry and Coordinate System

the constitutive matrix is based on an Eulerian coordinate system. This is assumed to be an accurate relationship if the strains are small, even with large displacements and rotations. 7) The theory assumes that an individual fiber-matrix "cube" is transversly isotropic, but a laminae of unidirectional fibers in a matrix behaves orthotropically.

2.1.2 Background.   There are several key elements to the SLR theory which describe its uniqueness and usefulness. Since a shell has curvature, a curvilinear coordinate system is used. The coordinates for curvature in two directions are shown in Figure 2.1 (5). For this work, however, a cylinder is assumed. Therefore, the following references from Figure 2.2 are used (5).

$$\xi_1 \ = \ x \qquad (R_1 = \infty)$$

Figure 2.2   Cylindrical Shell Reference Geometry and Coordinate System

$$\xi_2 \ = \ s \qquad (R_2 = R) \qquad\qquad (2.1)$$

$$\zeta \ = \ z$$

Green's strain tensor is developed and reported in pp. 22-26 of (5). For the stress and strain tensors, a shorthand notation is listed in Table 2.1. A modified representation, based on the shell assumptions, is used in the SLR theory. First, it is assumed ϵ_3 is approximately zero. This assumption is valid since the thickness of the laminate will not vary significantly during loading. Because of the thin shell assumptions, it is reasonable to assume the in-plane stresses and strains are more dominant than the transverse stresses and strains. Therefore, the full Green's representation of the in-

Table 2.1   Shorthand Tensor Notation

STRESS	STRAIN	COORDINATES
$\sigma_{11} = \sigma_1$	$\epsilon_{11} = \epsilon_1$	$X = 1$
$\sigma_{22} = \sigma_2$	$\epsilon_{22} = \epsilon_2$	$S = 2$
$\sigma_{33} = \sigma_3$	$\epsilon_{33} = \epsilon_3$	$Z = 3$
$\sigma_{23} = \sigma_4$	$2\epsilon_{23} = \epsilon_4$	$SZ = 4$
$\sigma_{13} = \sigma_5$	$2\epsilon_{13} = \epsilon_5$	$XZ = 5$
$\sigma_{12} = \sigma_6$	$2\epsilon_{12} = \epsilon_6$	$XS = 6$

plane strains, $(\epsilon_1, \epsilon_2,$ and $\epsilon_6)$, are developed, while the linear terms for the transverse strains, $(\epsilon_4$ and $\epsilon_5)$, are used. This abridged representation of the strains yields a breakdown in continuity, especially for the transverse shear strains. However, for problems of moderate to small rotations, the continuity equations are approximately met. The compatibility equations are satisfied for the linear case where only small displacement and rotations exist (5).

For the SLR theory, as for the Reissner-Mindlin (RM) (3),(4) theories, plane sections are not required to remain normal to the midplane. This allows both a bending rotation and a transverse shear deflection. The out-of-plane motion of the element is not captured merely by the change in slope of the w component, but also by an additional rotation degree of freedom, Ψ. This rotation exists in the x and s directions.

2.1.3 Kinematics.

As mentioned, the transverse strains assume a parabolic relationship through the thickness. This representation accounts for an internal transverse shear which reduces to zero on the upper and lower surfaces. In order to develop these strains in the laminate, it is important to capture the proper kinematics through the displacement terms. Applying the SLR kinematics to a cylindrical shell results in the following representation for the u, v, and w displacements (5):

$$
\begin{aligned}
u(x, s, z) &= u_0 + z\Psi_x - \frac{4}{3h^2}z^3(\Psi_x + w_{,x}) \\
v(x, s, z) &= v_0(1 - \frac{z}{R}) + z\Psi_s - \frac{4}{3h^2}z^3(\Psi_s + w_{,s}) \\
w(x, s) &= w
\end{aligned}
\tag{2.2}
$$

where h is the total laminate thickness, u_0 and v_0 are measured at the midplane, and z is the distance from the midplane. These kinematics were derived from a Taylor's series expansion for the z-direction about the midplane. This approach was first used

for a shell by Bassett (40). The differences in many of the shell and plate theories depends on the chosen truncation of this infinite series.

Shear locking is a problem in RM kinematics. As the thickness decreases, bending dominates over the shear. In RM theories, the shear and bending terms are the same order, which results in a disproportionate representation. The shear terms form a "penalty matrix" (41). This penalty matrix overconstrains the finite element analysis, causing it to "lock." In the SLR theory, there is a higher order representation of the shear terms, which reduce to zero as the thickness decreases. Therefore, the bending terms are allowed to dominate for a thin model and shear locking is avoided.

2.1.4 *Elasticity relations.*

The above kinematics are applied to the Green strain-displacement relations listed in (5). As mentioned above, the full Green strain representation is used for the in-plane strains, the transverse strains are linear in displacement, and ϵ_3 is assumed negligible. The in-plane strains become:

$$
\begin{aligned}
\epsilon_1 &= \underline{\epsilon}_1^0 + z\kappa_1 + z^2\kappa_1^2 + z^3\kappa_1^3 + z^4\kappa_1^4 + z^6\kappa_1^6 \\
\epsilon_2 &= \underline{\epsilon}_2^0 + z\kappa_2 + z^2\kappa_2^2 + z^3\kappa_2^3 + z^4\kappa_2^4 + z^6\kappa_2^6 \\
\epsilon_6 &= \underline{\epsilon}_6^0 + z\kappa_6 + z^2\kappa_6^2 + z^3\kappa_6^3 + z^4\kappa_6^4 + z^6\kappa_6^6
\end{aligned} \tag{2.3}
$$

where $\underline{\epsilon}_J^0$ (J=1, 2, 6) are the respective midplane strains and the κ_J^I (J=1, 2, 6), (I=1, 2, 3, 4, 6) are individual strain components corresponding to the Ith power of z (yet, the κ_J^I are not raised to a power). These values are shown in Appendix A of (5). The transverse shearing strains are:

$$
\begin{aligned}
\epsilon_4 &= \frac{1}{1 - \frac{z}{R}}(w_{,s} + \Psi_s)(1 - \frac{4z^2}{h^2}) \\
\epsilon_5 &= (w_{,x} + \Psi_x)(1 - \frac{4z^2}{h^2})
\end{aligned} \tag{2.4}
$$

One should note the parabolic through-the-thickness representation of the ϵ_4 and ϵ_5 strains. Also, the transverse strains are zero at the top and bottom surfaces, $(\frac{h}{2}, \frac{-h}{2})$.

In shorthand notation, the strains can be represented by:

$$\epsilon_i^0 + z^p \kappa_{ip} \tag{2.5}$$

where i=1, 2, 6 and p=1, 2, 3, 4, 5, 6, 7 (See (5), equation (2.48-49) for derivation of this expression).

Finally, all the necessary degrees of freedom have been introduced, $[u, v, w, w_{,x}, w_{,s}, \Psi_x, \Psi_s]$, where the comma-subscript denotes derivative with respect to the subscript.

The constitutive relationship for an orthotropic unidirectional laminae is given in (1) as:

$$
\begin{Bmatrix}
\sigma_1 \\
\sigma_2 \\
\sigma_3 \\
\sigma_4 \\
\sigma_5 \\
\sigma_6
\end{Bmatrix}
=
\begin{bmatrix}
C_{11} & C_{12} & C_{13} & 0 & 0 & 0 \\
C_{12} & C_{22} & C_{23} & 0 & 0 & 0 \\
C_{13} & C_{23} & C_{33} & 0 & 0 & 0 \\
0 & 0 & 0 & C_{44} & 0 & 0 \\
0 & 0 & 0 & 0 & C_{55} & 0 \\
0 & 0 & 0 & 0 & 0 & C_{66}
\end{bmatrix}
\begin{Bmatrix}
\epsilon_1 \\
\epsilon_2 \\
\epsilon_3 \\
\epsilon_4 \\
\epsilon_5 \\
\epsilon_6
\end{Bmatrix}
\tag{2.6}
$$

where C_{ij} is a function of the material properties $E_1, E_2, G_{12}, G_{13}, G_{23}, \nu_{12}, \nu_{21}$, and ν_{23}. E_i is the Young's modulus, G_{ij} is the shear modulus, and ν_{ij} is the Poisson's ratio, all in the respective directions. The σ_3 component is assumed to be zero. This representation allows for an ϵ_3. It order to eliminate this term, line three of the above equation is solved for ϵ_3:

$$\epsilon_3 = -\frac{C_{13}}{C_{33}}\epsilon_1 - \frac{C_{23}}{C_{33}}\epsilon_2 \tag{2.7}$$

This expression is then redistributed to the other terms, eliminating ϵ_3:

$$
\left\{ \begin{array}{c} \sigma_1 \\ \sigma_2 \\ \sigma_6 \\ \sigma_4 \\ \sigma_5 \end{array} \right\} = \left[\begin{array}{ccccc} Q_{11} & Q_{12} & 0 & 0 & 0 \\ Q_{12} & Q_{22} & 0 & 0 & 0 \\ 0 & 0 & Q_{66} & 0 & 0 \\ 0 & 0 & 0 & Q_{44} & 0 \\ 0 & 0 & 0 & 0 & Q_{55} \end{array} \right] \left\{ \begin{array}{c} \epsilon_1 \\ \epsilon_2 \\ \epsilon_6 \\ \epsilon_4 \\ \epsilon_5 \end{array} \right\} \qquad (2.8)
$$

where

$$
Q_{ij} = C_{ij} - \frac{C_{i3}C_{j3}}{C_{33}}
$$

These terms yield:

$$
\begin{aligned}
Q_{11} &= \frac{E_1}{\Delta} \\
Q_{12} &= \frac{\nu_{12}E_2}{\Delta} \\
Q_{22} &= \frac{E_2}{\Delta} \\
Q_{66} &= G_{12} \\
Q_{44} &= G_{23} \\
Q_{55} &= G_{13}
\end{aligned} \qquad (2.9)
$$

where

$$
\Delta = 1 - \nu_{12}\nu_{21}
$$

For a multidirectional laminate, the constitutive equations for each ply must be transformed into the global coordinate system. This is done through the following

2-7

transformation:

$$
\left\{ \begin{array}{c} \sigma_1 \\ \sigma_2 \\ \sigma_6 \\ \sigma_4 \\ \sigma_5 \end{array} \right\} = [T^*] \begin{bmatrix} Q_{11} & Q_{12} & 0 & 0 & 0 \\ Q_{12} & Q_{22} & 0 & 0 & 0 \\ 0 & 0 & Q_{66} & 0 & 0 \\ 0 & 0 & 0 & Q_{44} & 0 \\ 0 & 0 & 0 & 0 & Q_{55} \end{bmatrix} [T^*]^T \left\{ \begin{array}{c} \epsilon_1 \\ \epsilon_2 \\ \epsilon_6 \\ \epsilon_4 \\ \epsilon_5 \end{array} \right\} \tag{2.10}
$$

This requires a tensoral transformation. Recall from Table 2.1, the current shorthand representation of the strain is not tensoral. Therefore, the strain is converted into tensoral strain, transformed, and then converted back to shorthand notation. The transformation matrix $[T^*]$ is then developed by:

$$
[T^*] = [R][T][R^*] \tag{2.11}
$$

where

$$
[R] = \begin{bmatrix} 1 & 0 & 0 & 0 & 0 \\ 0 & 1 & 0 & 0 & 0 \\ 0 & 0 & 2 & 0 & 0 \\ 0 & 0 & 0 & 2 & 0 \\ 0 & 0 & 0 & 0 & 2 \end{bmatrix}
$$

$$
[T] = \begin{bmatrix} c^2 & s^2 & -2cs & 0 & 0 \\ s^2 & c^2 & 2cs & 0 & 0 \\ cs & -cs & (c^2 - s^2) & 0 & 0 \\ 0 & 0 & 0 & c^2 & -s^2 \\ 0 & 0 & 0 & s^2 & c^2 \end{bmatrix}
$$

$$[R^*] = \begin{bmatrix} 1 & 0 & 0 & 0 & 0 \\ 0 & 1 & 0 & 0 & 0 \\ 0 & 0 & \frac{1}{2} & 0 & 0 \\ 0 & 0 & 0 & \frac{1}{2} & 0 \\ 0 & 0 & 0 & 0 & \frac{1}{2} \end{bmatrix}$$

and

$$c = \cos(\Phi) \qquad s = \sin(\Phi) \qquad \Phi=\text{fiber orientation}$$

The equations resulting from this transformation can be broken into in-plane and transverse portions:

$$\left\{ \begin{array}{c} \sigma_1 \\ \sigma_2 \\ \sigma_6 \end{array} \right\} = \begin{bmatrix} \overline{Q}_{11} & \overline{Q}_{12} & \overline{Q}_{16} \\ \overline{Q}_{12} & \overline{Q}_{22} & \overline{Q}_{26} \\ \overline{Q}_{16} & \overline{Q}_{26} & \overline{Q}_{66} \end{bmatrix} \left\{ \begin{array}{c} \epsilon_1 \\ \epsilon_2 \\ \epsilon_6 \end{array} \right\} \tag{2.12}$$

and

$$\left\{ \begin{array}{c} \sigma_4 \\ \sigma_5 \end{array} \right\} = \begin{bmatrix} \overline{Q}_{44} & \overline{Q}_{45} \\ \overline{Q}_{45} & \overline{Q}_{55} \end{bmatrix} \left\{ \begin{array}{c} \epsilon_4 \\ \epsilon_5 \end{array} \right\} \tag{2.13}$$

where the individual terms are:

$$\begin{aligned}
\overline{Q}_{11} &= Q_{11}c^4 + Q_{22}s^4 + 2Q_{12}c^2s^2 + 4Q_{66}c^2s^2 \\
\overline{Q}_{22} &= Q_{11}s^4 + Q_{22}c^4 + 2Q_{12}c^2s^2 + 4Q_{66}c^2s^2 \\
\overline{Q}_{12} &= Q_{11}c^2s^2 + Q_{22}c^2s^2 + Q_{12}(c^4 + s^4) - 4Q_{66}c^2s^2 \\
\overline{Q}_{16} &= Q_{11}c^3s - Q_{22}cs^3 + Q_{12}(cs^3 - c^3s) + 2Q_{66}(cs^3 - c^3s) \\
\overline{Q}_{26} &= Q_{11}cs^3 - Q_{22}c^3s + Q_{12}(c^3s - cs^3) + 2Q_{66}(c^3s - cs^3) \\
\overline{Q}_{66} &= Q_{11}c^2s^2 + Q_{22}c^2s^2 - 2Q_{12}c^2s^2 + Q_{66}(c^2 - s^2)^2
\end{aligned} \tag{2.14}$$

and

$$
\begin{aligned}
\overline{Q}_{44} &= Q_{44}c^2 + Q_{55}s^2 \\
\overline{Q}_{55} &= Q_{44}s^2 + Q_{55}c^2 \\
\overline{Q}_{45} &= Q_{44}cs - Q_{55}cs
\end{aligned}
\tag{2.15}
$$

again,

$$
c = \cos(\Phi) \qquad s = \sin(\Phi) \qquad \Phi = \text{fiber orientation}
$$

The transformed constitutive matrix coefficients are denote by a bar, $\overline{Q}_{ij}$. Note that the transformations are on a ply-by-ply basis, since each ply may contain a unique orientation. Later, these will be integrated over the thickness.

2.1.5 *Strain Energy.*   The potential energy of a shell is described as the internal strain energy plus the product of the external force and the respective displacements. This is abbreviated as:

$$
\Pi_p = U - V
\tag{2.16}
$$

In general, V can be determined by

$$
V = P_i u_i
$$

where P_i is a force vector component and u_i is the associated displacement component. The strain energy term can be represented by:

$$
U = \frac{1}{2} \int_V \sigma_i^T \cdot \epsilon_j dV
\tag{2.17}
$$

From equation (2.12), $\sigma_i = \overline{Q}_{ij}\epsilon_j$, and equation (2.17) can be written in terms of strain only. For convenience, the strain energy is broken into in-plane and transverse

energies:

$$U = U_1 + U_2$$

$$
\begin{aligned}
U_1 \;=\; & \frac{1}{2}\int_\Omega\int_h (\overline{Q}_{11}(\epsilon_1^0 + z^p\kappa_{1p})^2 + \overline{Q}_{22}(\epsilon_2^0 + z^p\kappa_{2p})^2 \\
& 2\overline{Q}_{12}(\epsilon_1^0 + z^p\kappa_{1p})(\epsilon_2^0 + z^r\kappa_{2r}) + \overline{Q}_{66}(\epsilon_6^0 + z^p\kappa_{6p})^2 \\
& 2\overline{Q}_{16}(\epsilon_1^0 + z^p\kappa_{1p})(\epsilon_6^0 + z^r\kappa_{6r}) \\
& 2\overline{Q}_{26}(\epsilon_2^0 + z^p\kappa_{2p})(\epsilon_6^0 + z^r\kappa_{6r}))dzd\Omega
\end{aligned}
\tag{2.18}
$$

$$
\begin{aligned}
U_2 \;=\; & \frac{1}{2}\int_\Omega\int_h (\overline{Q}_{44}(\epsilon_4^0 + z^2\kappa_{42})^2 + \overline{Q}_{55}(\epsilon_5^0 + z^2\kappa_{52})^2 \\
& 2\overline{Q}_{45}(\epsilon_4^0 + z^2\kappa_{42})(\epsilon_5^0 + z^2\kappa_{52}))dzd\Omega
\end{aligned}
\tag{2.19}
$$

where p, r = 1, 2, 3, 4, 5, 6, 7.

The evaluation of this expression is lengthy, and only the in-plane equations are shown. Similar terms are grouped as follows:

$$U_1 = \frac{1}{2}\int_\Omega (u_1 + u_2 + u_3)d\Omega \tag{2.20}$$

where

$$
\begin{aligned}
u_1 \;=\; & \int_h \epsilon_j^0\epsilon_i^0\overline{Q}_{ij}dz \\
\;=\; & \epsilon_j^0\epsilon_i^0 A_{ij} \tag{2.21} \\
u_2 \;=\; & \int_h 2\epsilon_j^0\overline{Q}_{ij}\kappa_{ip}z^p dz \\
\;=\; & 2\epsilon_j^0(\kappa_{i1}B_{ij} + \kappa_{i2}D_{ij} + \kappa_{i3}E_{ij} + \kappa_{i4}F_{ij} \tag{2.22} \\
& + \kappa_{i5}G_{ij} + \kappa_{i6}H_{ij} + \kappa_{i7}I_{ij}) \\
u_3 \;=\; & \int_h \kappa_{jp}\kappa_{ir}\overline{Q}_{ij}z^{p+r}dz \\
\;=\; & \kappa_{j1}\kappa_{i1}D_{ij} + 2\kappa_{j1}\kappa_{i2}E_{ij} + (2\kappa_{j1}\kappa_{i3} + \kappa_{j2}\kappa_{i2})F_{ij}
\end{aligned}
$$

$$+ 2(\kappa_{j1}\kappa_{i4} + \kappa_{j2}\kappa_{i3})G_{ij} + (2\kappa_{j1}\kappa_{i5} + 2\kappa_{j2}\kappa_{i4} + \kappa_{j3}\kappa_{i3})H_{ij}$$

$$+ 2(\kappa_{j1}\kappa_{i6} + \kappa_{j2}\kappa_{i5} + \kappa_{j3}\kappa_{i4})I_{ij} + (2\kappa_{j1}\kappa_{i7}$$

$$+ 2\kappa_{j2}\kappa_{i6} + 2\kappa_{j3}\kappa_{i5} + \kappa_{j4}\kappa_{i4})J_{ij} \qquad (2.23)$$

$$+ 2(\kappa_{j2}\kappa_{i7} + \kappa_{j3}\kappa_{i6} + \kappa_{j4}\kappa_{i5})K_{ij} + (2\kappa_{j3}\kappa_{i7}$$

$$+ 2\kappa_{j4}\kappa_{i6} + \kappa_{j5}\kappa_{i5})L_{ij} + (2\kappa_{j4}\kappa_{i7} + \kappa_{j5}\kappa_{i6})P_{ij}$$

$$+ 2\kappa_{j5}\kappa_{i7} + \kappa_{j6}\kappa_{i6})R_{ij} + 2\kappa_{j6}\kappa_{i7}S_{ij} + \kappa_{j7}\kappa_{i7}T_{ij}$$

and $i, j = 1, 2, 6$ and $p, r = 1, 2, 3, 4, 5, 6, 7$.

The elasticity arrays (A_{ij}, B_{ij}, etc.) are determined when the constitutive matrices are multiplied by different powers of z and integrated over the thickness, yielding:

$$[A_{ij}, B_{ij}, D_{ij}, E_{ij}, F_{ij}, G_{ij}, H_{ij}, I_{ij}, J_{ij}, K_{ij}, L_{ij}, P_{ij}, R_{ij}, S_{ij}, T_{ij}] =$$
$$\int_h \overline{Q}_{ij}[1, z, z^2, z^3, z^4, z^5, z^6, z^7, z^8, z^9, z^{10}, z^{11}, z^{12}, z^{13}, z^{14}]dz \qquad (2.24)$$

where $i, j = 1, 2$, and 6. The first three terms are identical to the A_{ij}, B_{ij}, and D_{ij} matrices from classical laminate theory (42). The same procedures for the transverse equations produce:

$$U_2 = \frac{1}{2}\int_\Omega (\epsilon_m^0 \epsilon_n^0 A_{mn} + 2\epsilon_n^0 \kappa_{m2} D_{mn} + \kappa_{n2}\kappa_{m2} F_{mn})d\Omega \qquad (2.25)$$

and

$$[A_{mn}, D_{mn}, F_{mn}] = \int_h \overline{Q}_m n[1, z^2, z^4]dz \qquad (2.26)$$

where m, n = 4, 5. The elasticity arrays comprised of odd powers of z (e.g. B_{ij}, E_{ij}, G_{ij}, ..., S_{ij}) are eliminated if a symmetrical ply layup is assumed.

In FEM, the above integrations are performed numerically in a technique known as Gauss quadrature (41). In Gauss quadrature, the integration is evalu-

ated at certain points, known as Gauss points. If enough Gauss points are chosen, the numerical technique will accurately approximate the actual integration.

2.2 Finite Element Method

In statics, force and displacement are related by a stiffness coefficient. The simplistic equation that defines this relation is:

$$F = kd$$

where F is the force, k is the stiffness, and d is the displacement. This equation applies to a spring just as well as other continuum. In the previous section, the constitutive relationship between stress and strain was introduced. Generally speaking, stress is a function of the force, and strain is a function of displacement. Therefore, the constitutive matrix is analogous to the stiffness coefficient, k.

In the previous section, the potential energy functional, Π_p, was also introduced. It was comprised of the strain energy (a relation of stress and strain) and the applied force times displacement. Again, the force, displacement, and stiffness terms are prevalent throughout. In this way, the potential energy of the continuum can be used to solve the response to displacements and/or forces. This problem and others can be represented by differential equations (known as the strong form) or integral equations (known as the weak form) (41). The conditions of the strong form must be met everywhere, while conditions of the weak form must be met only in an average sense.

A functional, such as the potential energy, is an integral expression of the differential equations that govern a problem. Therefore, a functional is in the weak form. For a functional to represent a problem, it must satisfy three things:

1. Boundary conditions.

2. Compatibility.

3. Equilibrium.

Examples of each for a statics problem are as follows: If the end of a continuum is clamped to a rigid structure, the functional must not allow answers containing displacements at that point. This is an example of a boundary condition. Also, a functional that yields a discontinuous solution, such as having a jump or separation, violates compatibility for the continuum. If equilibrium is not met, the result would imply that forces are not balanced.

For a simple rod, it might be possible to directly solve the equation $F = kd$. Most problems, however, are just too complex. Therefore, the geometry of the continuum is broken into discrete, or finite, representations. It is now possible to solve for each discrete element, and then sum the response over the entire continuum. While each element may not meet all the necessary criteria, it is possible to meet the above conditions on an average sense over the entire continuum.

2.2.1 Building the Finite Element.

The FEM model that represents the SLR theory is a 36 degree-of-freedom curved rectangular element, shown in Figure 2.3 (5). The corner, or vertex, nodes have seven degrees of freedom, $[u, v, w, w_{,x}, w_{,s}, \Psi_x, \Psi_s]$. There are four "mid-side" nodes with degrees of freedom u and v. In order to define the degrees of freedom along the edges of the element, the displacements or rotations are *interpolated* between the nodes. The type of function used for interpolation regulates the level of continuity obtainable. The notation C^m is used, where the mth derivative of the function is continuous (41). For example, if the function ϕ has C^0 continuity, ϕ is continuous, but its derivative, $\frac{d\phi}{dx}$ is not. C^0 continuity is sufficient for extension, since only the displacements are required to be continuous. Bending rotation is defined by a slope, which is developed by a derivative of the w degree-of-freedom. Therefore, C^1 continuity is required for bending deflection. For the present theory, only C^0 continuity is required for the
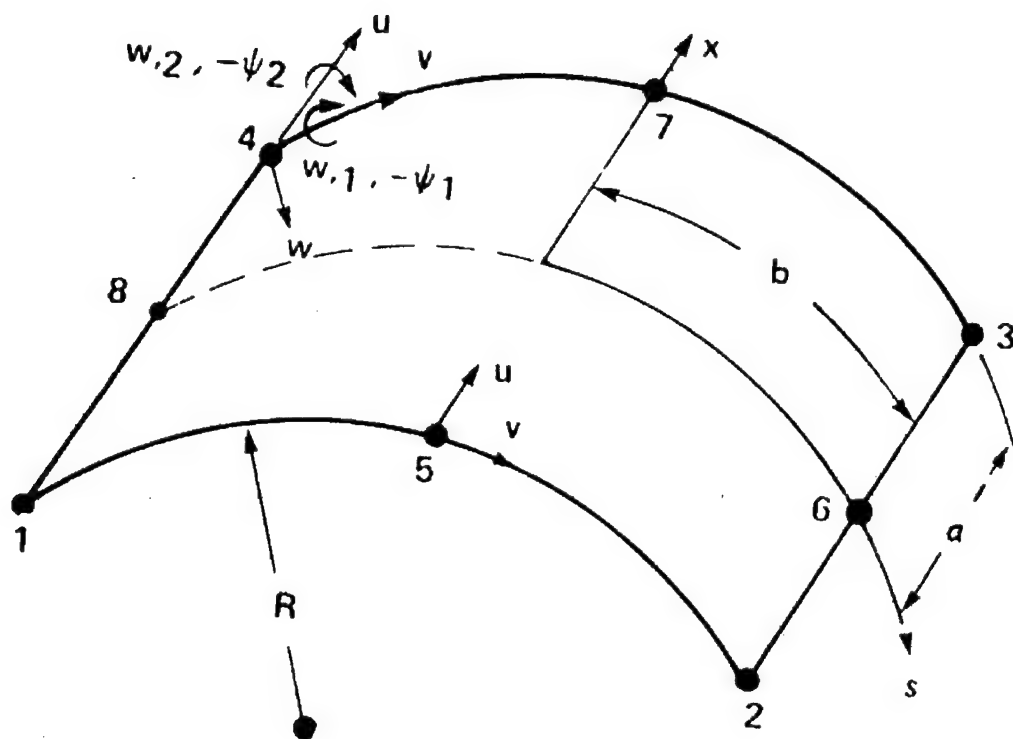
Figure 2.3   36 DOF Finite Element for SLR Theory

displacement degrees-of-freedom, u, v, Ψ_x, and Ψ_s. Degrees-of-freedom $w, w_{,x}, w_{,s}$ define bending deflection and require C^1 continuity.

The degrees of freedom are interpolated by multiplying a matrix of shape functions by an array containing the degrees of freedom. The shape functions must meet the boundary conditions at the nodes, while representing the proper interpolation between nodes. There are various types of shape functions. Since only C^0 continuity is required for u, v, Ψ_x, Ψ_s, a linear or Lagrangian shape function may be used. However, since the u and v displacements for a shell are quite complex, it is best to use higher order shape functions (5). A quadratic representation provides more accuracy. For w and its slopes, a *Hermitian* shape function imparts C^1 continuity.

A finite element is usually established in its own internal coordinate system. The relationship between the finite element coordinate system and the global system is a *Jacobian* matrix, J. The Jacobian is found by using chain-rule differentiation between coordinate systems (41). Now, the physical displacements, d, can be written in terms of the elements degrees of freedom, q (5):

$$\{d\} = [\Gamma][D]\{q\} \tag{2.27}$$

where

$$\{d\}^T = [u, u_{,1}, u_{,2}, v, v_{,1}, v_{,2}, w, w_{,1}, w_{,2}, w_{,11}, w_{,22}, w_{,12}, \Psi_1, \Psi_{1,1}, \Psi_{1,2}, \Psi_2, \Psi_{2,1}, \Psi_{2,2}]$$

$$[\Gamma] = [J]^{-1}$$

$$[D] = \text{Shape functions}$$

$$\{q\} = 36 \text{ DOF element array}$$

where $\{q\}$ is a 36x1 array, $[D]$ is an 18x36 matrix, $[\Gamma]$ is an 18x18 matrix, and $\{d\}$ is an 18X1 array.

2.2.2 Applying the Potential Energy to Finite Element Analysis.

The potential energy representation, Π_p, for the SLR theory is (5):

$$\Pi_p = \frac{q^T}{2}(K + \frac{N_1}{3} + \frac{N_2}{6})q - q^T R \tag{2.28}$$

where K is a matrix of constant stiffness coefficients, N_1 is a matrix of stiffness coefficients that are a function of the displacement, N_2 is a matrix of stiffness coefficients that are a function of the displacement squared, and R is the force vector. If the stiffness coefficients are divided this way, the matrices are easier to manipulate. The first variation of this expression with respect to the degree of freedom array, $\{q\}$, using the calculus of variations, yields:

$$\delta\Pi_p = \delta q^T[(K + \frac{N_1}{2} + \frac{N_2}{3})q - R] = 0 \tag{2.29}$$

Since δq is an arbitrary value, and the trivial case $\delta q = 0$ is ignored, the equation in the bracket must equal zero to satisfy equilibrium:

$$(K + \frac{N_1}{2} + \frac{N_2}{3})q - R = 0 \tag{2.30}$$

Notice this is the simple equation for statics written at the beginning of this section, $F = kd$. The static behavior of an arbitrary shell has now been represented through finite element modeling.

Solving equation (2.30) is not easy, since N_1 and N_2 vary with the displacement, making the equation nonlinear. This equation is solved through the iterative Newton-Raphson (NR) technique, which is a powerful tool in computational analysis (41). For shorthand, let:

$$(K + \frac{N_1}{2} + \frac{N_2}{3})q - R = F(q)$$

A small increment is added to q and the Taylor's series expansion of $F(q + \Delta q) = 0$ is developed. The higher order terms are neglected (since Δq is small), yielding:

$$F(q + \Delta q) = F(q) + \frac{\partial F}{\partial q}\Delta q + \ldots = 0 \tag{2.31}$$

$$\frac{\partial F}{\partial q}\Delta q = -F(q) \tag{2.32}$$

If

$$F(q) = (K + \frac{N_1}{2} + \frac{N_2}{3})q - R$$

then

$$\frac{\partial F}{\partial q} = (K + N_1 + N_2) \tag{2.33}$$

remembering that $N_1 = f(q)$ and $N_2 = f(q^2)$.

$(K + N_1 + N_2)$ is the tangent stiffness matrix, denoted as K_T. Equation (2.32) can now be written:

$$K_T \Delta q = -F(q) \tag{2.34}$$

The current values of q are substituted into N_1 and N_2 of K_T, and equation (2.34) is solved for Δq. This value is added to q and the right-hand side (RHS) is updated. Remember that

$$F(q) = (K + \frac{N_1}{2} + \frac{N_2}{3})q - R$$

For the exact solution, $F(q)$ would equal zero. For FEM, the process is repeated until $F(q)$ reduces to a small value. This is done through a convergence check. While there are several ways to calculate convergence, the chosen method for the SLR FEM is:

$$\frac{\sqrt{\sum_i (q_r^i)^2} - \sqrt{\sum_i (q_{r-1}^i)^2}}{\sqrt{\sum_i (q_1^i)^2}} \times 100\% \leq TOL \tag{2.35}$$

where i is the degree of freedom number, r is the increment, and TOL is the tolerance value. A typical tolerance value is 0.1%. Once the tolerance is reached, the next increment of load or displacement is applied.

At this point it is important to note the difference between the increment, Δq, and the iteration. The problem is solved through incremental additions of the degrees of freedom, q. For each increment, equation (2.34) is iterated until tolerance is met. Once tolerance is met, the next increment is applied. In the Newton-Raphson approach, the tangent stiffness, K_T, (which is the slope of equilibrium curve at the point in question) is used to project forward. Other approaches use the initial stiffness or the secant stiffness. The initial stiffness is the linear stiffness and the secant stiffness is the slope of the line from the origin to the point in question. These approaches do not require calculation of the tangent stiffness each iteration, which is computationally more efficient. However, the initial and the secant stiffnesses do not take as large a step each iteration, requiring more iterations. The NR approach reduces the number of iterations required for convergence.

It is also important to note the described procedure is displacement control, where the displacements (or the degrees of freedom, q) are incremented. It is also possible to increment load, R, or even a combination of the two.

2.3 Failure Criteria

Failure criteria are a comparison of applied parameters to material allowable parameters. The parameter of choice is usually stress, but others such as strain or strain energy (43) are also used. According to Tsai (44), as reported by Spottswood (20), most failure criterion are classified as interactive or non-interactive. A non-interactive criterion does not consider multiple parameter interactions, examples of which are the maximum stress and maximum strain theories. A non-interactive criterion is best suited for brittle isotropic materials (20). An interactive criterion attempts to account for load combinations.

The ultimate values of a stress failure criterion can be plotted in the stress plane. The maximum, or constant, stress criterion is a rectangular block, which
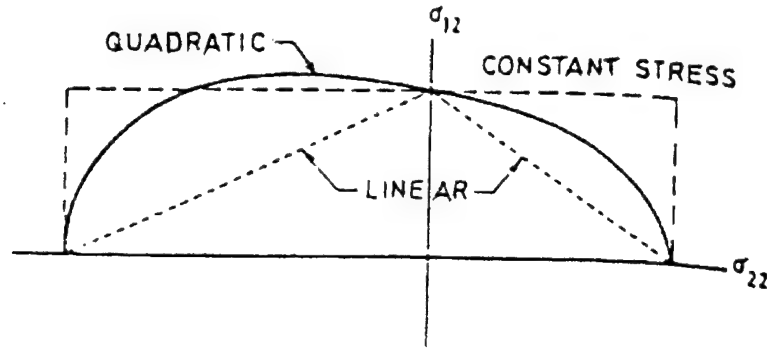
Figure 2.4   Failure Surfaces for Various Failure Approximations

overestimates the biaxial stress interactions as shown in Figure 2.4 (16). A linear criterion will underestimate the cross-ply stress. A quadratic curve fit is a better approximation of the material strengths, and higher order approximations increase complexity but do little to improve the fit. A smooth quadratic curve works well for isotropic materials, but difficulties are introduced when applied to composite materials due to their different failure modes (16). The smooth curve does not distinguish between different failure modes and will therefore result in an incompatible expression in regions of failure mode interaction. In order to use a quadratic failure expression, and yet consider the different failure modes of composites, a piecewise smooth criterion was developed by Hashin (16). Each smooth curve represents a composite laminate failure mode.

The basis for the Hashin criteria is the transverse isotropic properties of a fiber-matrix composite. If the criterion is to model the actual material, it must also exhibit transverse isotropy—that is, it must be invariant in rotations around the fiber, or x_1, axis. The failure criterion is thus based on the following stress invariants for a composite material (16):

$$I_1 = \sigma_{11}$$

$$I_2 = \sigma_{22} + \sigma_{33}$$

$$I_3 = \sigma_{23}^2 - \sigma_{22}\sigma_{33} \tag{2.36}$$

$$\text{or} \quad I_3 = \frac{1}{4}(\sigma_{22} - \sigma_{33})^2 + \sigma_{23}^2$$

$$I_4 = \sigma_{12}^2 + \sigma_{13}^2$$

$$I_5 = 2\sigma_{12}\sigma_{23}\sigma_{13} - \sigma_{22}\sigma_{13}^2 - \sigma_{33}\sigma_{12}^2$$

In the transverse-isotropic model, the 1 direction is aligned with the fiber. Only quadratic terms are desired, and the cubic term, I_5, is discarded. The resulting invariants are then combined to form the general representation of the failure criteria:

$$A_1 I_1 + B_1 I_1^2 + A_2 I_2 + B_2 I_2^2 + C_{12} I_1 I_2 + A_3 I_3 + A_4 I_4 = 1 \tag{2.37}$$

The factors A_i, B_i, and C_{ij} are determined depending on the type of material strength corresponding to the invariants.

2.3.1 Fiber Failure.

Fiber failure in tension is assumed to not depend on σ_{22}, σ_{33}, or σ_{23}, which are matrix dominated properties. For fiber failure in tension:

$$B_1 = \frac{1}{\sigma_{FN}^2} \quad \text{and} \quad A_4 = \frac{1}{\sigma_{FS}^2}$$

where

$$\sigma_{FN} = \text{Ultimate Fiber Failure in Tension Stress}$$

$$\sigma_{FS} = \text{Ultimate Fiber Failure in Shear}$$

and all other terms are assumed to be zero. This leads to the expression where fiber failure in tension occurs if:

$$\left(\frac{\sigma_{11}}{\sigma_{FN}}\right)^2 + \frac{(\sigma_{12}^2 + \sigma_{13}^2)}{\sigma_{FS}^2} \geq 1 \tag{2.38}$$

In order to use the failure criterion, it is necessary to perform experimental tests to determine individual failure properties. Fortunately, these values have been determined for most composite materials.

2.3.2 Matrix Failure.

It is assumed that the fiber carries the longitudinal stress, σ_{11}, so this factor is not present in the matrix failure criterion. Equation (2.37) is reduced to:

$$A_2 I_2 + B_2 I_2^2 + A_3 I_3 + A_4 I_4 = 1 \qquad (2.39)$$

Matrix failure is divided into two types: tension and compression. For the tension case, the factors in equation (2.39) are determined. First, A_2 is deleted in favor of the quadratic term B_2. Tensile loading for the matrix occurs in either the 2 or 3 direction, so

$$
\begin{aligned}
B_2 &= \frac{1}{\sigma_{MNT}^2} \\
A_3 &= \frac{1}{\sigma_{MS}^2} \\
A_4 &= \frac{1}{\sigma_{FS}^2}
\end{aligned}
$$

and the matrix tension criterion is:

$$\frac{(\sigma_{22} + \sigma_{33})^2}{\sigma_{MNT}^2} + \frac{(\sigma_{23}^2 - \sigma_{22}\sigma_{33})}{\sigma_{MS}^2} + \frac{(\sigma_{12}^2 + \sigma_{13}^2)}{\sigma_{FS}^2} \geq 1 \qquad (2.40)$$

The compression case is more complicated. First a simple unidirectional compression loading is considered and an expression is determined in terms of A_2 and B_2. Then, the case where σ_{22} and σ_{33} are equally applied in compression is analyzed (again, ignoring the shearing terms of I_3 and I_4), resulting in another expression for A_2 and B_2. These two variables are then solved for by these two equations.

In the resulting expressions for these two variables, the terms above first-order are discarded. The resulting values are then applied to equation (2.39), which becomes:

$$\frac{[(\frac{\sigma_{MNC}}{2\sigma_{MS}})^2 - 1](\sigma_{22} + \sigma_{33})}{\sigma_{MNC}} + \frac{(\sigma_{22} - \sigma_{33})^2}{4\sigma_{MS}^2} + \frac{(\sigma_{23}^2 - \sigma_{22}\sigma_{33})}{\sigma_{MS}^2} + \frac{(\sigma_{12}^2 + \sigma_{13}^2)}{\sigma_{FS}^2} \geq 1 \quad (2.41)$$

where

$$\sigma_{MNT} = \text{Ultimate Matrix Failure in Tension}$$

$$\sigma_{MS} = \text{Ultimate Matrix Failure in Shear}$$

$$\sigma_{MNC} = \text{Ultimate Matrix Failure in Compression}$$

2.3.3 Delamination.

Delamination between the plies can also be assessed. The criterion is:

$$\frac{(\sigma_{23}^2 + \sigma_{13}^2)}{\sigma_{DS}^2} \geq 1 \quad (2.42)$$

where

$$\sigma_{DS} = \text{Ultimate Delamination Shear Strength}$$

This does not include the transverse normal stress, σ_{33}, which should be incorporated for a more accurate determination of delamination. Recall, however, that in the SLR theory, $\sigma_{33} = \sigma_3$, which is assumed to be zero. This factor is then not added to the failure criteria.

2.3.4 Maximum Strain Failure Criterion.

The need for a strain-based failure criterion is evident from the fatigue results, discussed in Chapter 4. A simple strain-based criterion is the maximum strain failure criterion. For this criterion, failure occurs once the internal strain exceeds the material ultimate strain. For the fiber direction:

$$\frac{\epsilon_1}{\epsilon_N} \geq 1 \quad (2.43)$$

For the matrix direction:

$$\frac{\epsilon_2}{\epsilon_T} \geq 1 \qquad\qquad (2.44)$$

where

$$\epsilon_N \;=\; \text{Ultimate Strain in the 1-Direction}$$

$$\epsilon_T \;=\; \text{Ultimate Strain in the 2-Direction}$$

While not as exact as a quadratic criterion such as Hashin, it does identify the upper limit of strain failure.

2.4 *Stiffness Reduction*

Jamison and Reifsnider (31) identified three distinct stages of stiffness reduction in a graphite epoxy, $[0/90_2]_s$, laminate as shown in Figure 2.5. Stinchcomb and Bakis (30) comment on these stages, stating that Stage I is an rapid initial decrease primarily due to matrix cracking and some minor fiber failure. This is where the characteristic damage state (CDS) occurs. The CDS is defined as matrix cracking in the transverse plies, which eventually saturate and stabilize (23). Stage II is described by Stinchcomb and Bakis as "an intermediate but long period of stiffness reduction which results from additional matrix cracking in off-axis and on-axis plies, crack coupling along ply interfaces, and internal delaminations" (30). This correlates with the fatigue work of Talreja (24), also noted in Chapter 1. In Figure 2.5, it is observed that during Stage II the stiffness reduction is approximately linear with the number of cycles. Finally, Stage III occurs at the end of the fatigue life, and is due to large delaminations and/or fiber failures. The damage mechanisms are correlated to fatigue life through Figure 2.6 (30). Poursartip et al. (45) also show similar results for quasi-isotropic materials, especially for the initial Stage I drop and the approximately linear Stage II reduction in stiffness with number of cycles.
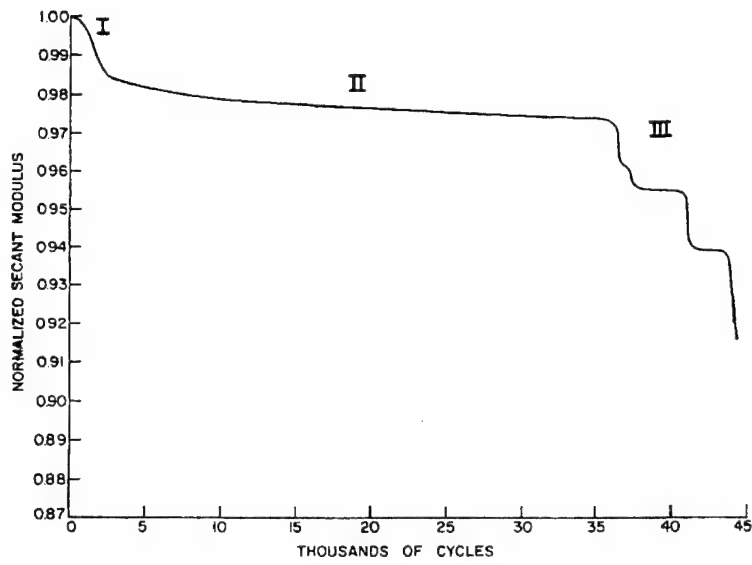
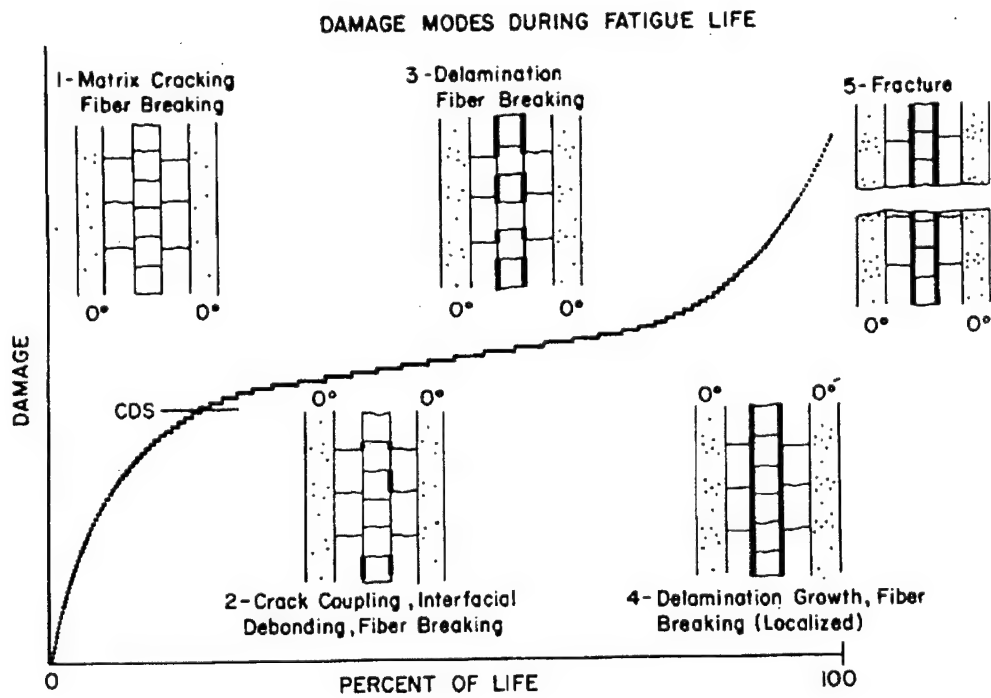Figure 2.5   Stiffness Reduction Due to Fatigue of a $[0/90_2]_s$ Graphite Epoxy Laminate

Figure 2.6   Damage Development During Fatigue Life of a Composite Laminate
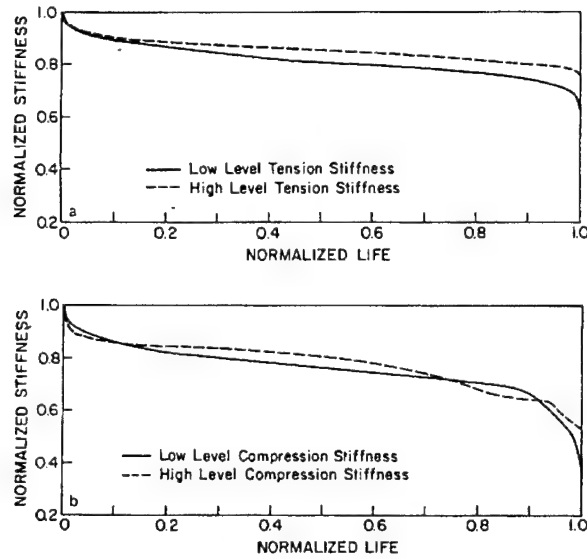
Figure 2.7   Normalized Stiffness vs. Fatigue Life for High and Low Fatigue Loads

Some interesting results regarding fatigue and stiffness reduction are noted by these authors. Their experiments involved 32-ply T300/5208 graphite epoxy quasi-isotropic laminates (28). For fatigue loads near 45% of the static strength, fatigue lives were on the order of 450,000 cycles to runout at 2,600,000 cycles. Fatigue loads near 55% of the static strength resulted in fatigue lives only around 100,000 cycles. Yet, for all these different tests, Stage I stiffness reduction occurs through 10-15% of the fatigue life and Stage III begins at 90-95% of the fatigue life. It seems, then, stiffness reduction is a favorable parameter to use in characterizing fatigue in composites. In fact, Stinchcomb and Bakis (30) show in Figure 2.7 that at both low and high fatigue loads, the change in the stiffness correlates directly to percentage of fatigue life (28).

It is important to discuss the effects loading and unloading have on the stress-strain curve, since this will affect the stiffness. Agarwal and Broutman (22) state if a composite material is loaded above its matrix cracking threshold, a change in stiffness will occur (22). Unloading occurs along a straight line, but one with a slope different than the initial stiffness. This unloading will result in a residual strain,

much like an elastic-plastic model for an isotropic material. Unlike elastic-plastic modeling, however, this residual strain will reduce to near zero upon increasing numbers of cycles. This result is also proven by Tahiri et al. (39) in plotting σ_{12} vs. ϵ_{12}. They show a build-up of residual strain for quasi-static loading involving two or three cycles. Next, the initial stress-strain slope is compared with one at 95% of the fatigue life. Both slopes originate from the same value of strain (and the residual strain is no longer present), but the latter slope is reduced from the initial value by about 19%.

III. Numerical Approach

Finite element analysis is a powerful tool to solve complicated problems by breaking them into smaller, easier-to-handle elements. There are several techniques which allow each analysis to be tailored to the problem at hand. It is important, however, that the finite element approach—at least on a global or average sense—approximate the physical results. For this research, some of the key factors in the finite element analysis are: 1) the boundary conditions and inputs, 2) application of the failure criterion, 3) iterating on damage, 4) reducing the stiffness to account for fatigue, and 5) the finite element model.

3.1 Boundary Conditions and Inputs

The boundary conditions for a static problem are its constraints, applied displacements, and applied tractions. In order for the model to behave as the actual structure does, the proper constraints must be enforced. Constraints are usually considered degrees of freedom that are fixed at zero. In the Finite Element Method (FEM), for example, if an edge is to be clamped, then the degrees of freedom of the nodes along the edge are forced to be zero.

The inputs are what cause the structure to displace, and hence cause internal strains and stresses to develop. For static problems, the two most common types of inputs are displacements and forces. The forces and the displacements are proportional to the stresses and strains, respectively. Therefore, an equilibrium relationship exists between force and displacement, just as it does for stress and strain. For linear problems, once one is applied the other may be found through the linear relationship. As mentioned in Chapter 2, for nonlinear problems, each resulting equilibrium point is based on the previous equilibrium point, and an incremental approach is required. It is very important in nonlinear problems whether the inputs are displacements,
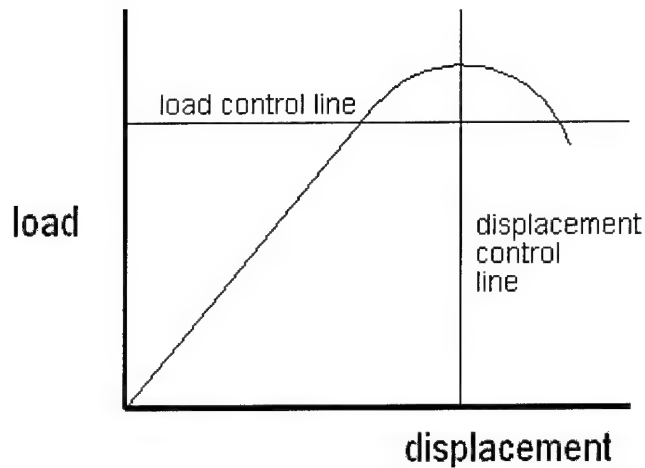
Figure 3.1   Load and Displacement Control

forces, or a combination of both, as the equations must be developed in a way to accommodate the type of input. When displacements are applied, it is known as displacement control, and when forces are applied, it is known as load control. The necessity to use one approach or the other is developed when two values may result for one input. This is evident in Figure 3.1. For an applied load (the load control line), there are two equilibrium points. The second point will never be reached by this method. The displacement control line easily traverses the maximum point and accurately determines the ultimate load. Combinations of load and displacement control, such as the Riks-Wempner approach (5), are much more complicated.

3.2   Applying the Failure Criterion

The Hashin failure criterion is easily applied to the finite element analysis, as described by Spottswood (20). The first step in the finite element analysis is the application of the boundary conditions and inputs. The solution is then iterated using the Newton-Raphson technique until equilibrium for that increment is reached. The degrees of freedom, (also referred to as the displacements, even though they contain

rotations as well) are now known for the given increment. These displacements are converted into strain using the strain-displacement relations. In the SLR code, this is performed in the STRESS subroutine, which may be called for every element. The strain is determined at the four outermost or "corner" Gauss points for every ply. This is done through nested loops, where the outer loop progresses through the plies while the inner loop counts through the four Gauss points within a ply. The strains are then converted into stresses through the constitutive relationships, again inside the nested loops. These stresses may then be displayed to the output file at each Gauss point at every ply in every element.

The material strengths for the given composite are determined in the local axis, based on a unidirectional fiber laminae. The stresses must be transformed into each ply's local axis for comparison with the material strengths through the failure criterion. A permanent flag is raised if the failure criterion is exceeded, allowing the accumulation of damage through the increments.

For the model to simulate actual damage, it must become more flexible as damage occurs. This is done through the reduction of the constitutive terms. Just as terms in the general Hashin criterion are tailored to the component evaluated, the element stiffness terms are reduced depending on the type of failure. Recall equation (2.8):

$$
\left\{
\begin{array}{c}
\sigma_1 \\
\sigma_2 \\
\sigma_6 \\
\sigma_4 \\
\sigma_5
\end{array}
\right\}
=
\left[
\begin{array}{ccccc}
Q_{11} & Q_{12} & 0 & 0 & 0 \\
Q_{12} & Q_{22} & 0 & 0 & 0 \\
0 & 0 & Q_{66} & 0 & 0 \\
0 & 0 & 0 & Q_{44} & 0 \\
0 & 0 & 0 & 0 & Q_{55}
\end{array}
\right]
\left\{
\begin{array}{c}
\epsilon_1 \\
\epsilon_2 \\
\epsilon_6 \\
\epsilon_4 \\
\epsilon_5
\end{array}
\right\}
\tag{2.8}
$$

The fiber is the key reinforcing element in a composite, and it dominates the properties in the axial direction. In the material axis for a unidirectional laminae,

the 1-direction is oriented with the fiber. Therefore, fiber failure affects all properties that involve the 1 direction, which are Q_{11}, Q_{12}, Q_{55}, and Q_{66}. These terms are reduced if fiber failure occurs. This is for tension only, since fiber failure due to compression is a complicated failure mechanism and dependent on the micromechanical interaction with the matrix (16). Fiber failure in compression is not considered.

Matrix failure is considered in tension and in compression. Once failure occurs, however, the result is the same. The terms Q_{22}, Q_{12}, Q_{44}, and Q_{66} are reduced accordingly. It is observed that failure to one constituent (e.g. matrix) does not "zero out" an element, but it is still able to carry load through the other constituent (e.g. fiber). This is one benefit of composite materials, and modeling them in this way is more appropriate.

Application of the delamination failure criterion is more involved. Delamination occurs between plies, but the stresses are only measured in the middle of a ply. Since σ_3 is ignored in the SLR theory, the delamination stresses are the two transverse shear stresses, σ_4 and σ_5. If these stresses exceed the criterion, delamination is assumed to occur between the plies. This is an approximation, but valid within the shell theory's parabolic representation of the transverse shearing stress. The parabolic representation ensures that if the stress at the middle of the ply exceeds the criterion, the stress for at least one of the interfaces will also exceed the criterion. This is true for a symmetric layup. If there is a single middle ply in the layup, the parabolic representation is a maximum at the middle of this ply and this reasoning breaks down. Even this case is considered negligible given the other assumptions, such as $\sigma_3 = 0$. As the shell thickness increases, the σ_3 component becomes more important. A code that accounts for the σ_3, includes the delamination effects of a free-edge, and determines the stresses at the ply interfaces is required for a more accurate determination of delamination between plies.

Delamination failure is modeled by reducing the Q_{44} and Q_{55} stiffness terms in the determining ply. If Q_{44} and Q_{55} are eliminated in a ply, the transverse shearing

stress cannot transmit across this ply. This is similar to a delamination between plies, which also prohibits the transverse shearing stress from crossing between plies.

The above procedures are also performed in the STRESS subroutine. First, the constitutive terms, Q_{ij}, are stored in dummy variables, AQ_{ij}, at the beginning of the subroutine. Then, in the inner loop of the STRESS subroutine, the failure criteria are applied at each Gauss point. If a criterion is exceeded, the appropriate dummy term is reduced to a small number. The term is not set exactly to zero, otherwise the stiffness matrix would become singular as the number of elements with damage increases. The arbitrary factor $\frac{1}{4000}$ is used in the program, as illustrated in this sample reduction:

$$AQ_{ij} = \frac{1}{4000}AQ_{ij}$$

Each AQ_{ij} term—whether it has been reduced or not—is divided by four, since this process occurs for each of the four Gauss points within a ply. These dummy variables are summed into another dummy variable TQ_{ij}, which is initialized to zero at the beginning of the STRESS subroutine:

$$TQ_{ij} = TQ_{ij} + \frac{AQ_{ij}}{4}$$

which is inside the inner Gauss point loop. If no failure occurred, the rebuilt constitutive term is equivalent to its original value. In this way, the constitutive term is reduced proportional to the amount of failure. For example, if failure occurred at two of the four Gauss points within a ply, TQ_{ij} would be approximately (ignoring the residual effect from the $\frac{1}{4000}$ multiplication) 50% of the original Q_{ij} value. This level of detail provides the opportunity for an accurate representation of actual composite material behavior. As before, these local constitutive terms are transformed into global coordinates and integrated through the thickness.

3.3 Iterating on Damage

In nonlinear finite element analysis, an incremental approach is required. For each increment, iterations are performed until equilibrium is reached. This incremental approach is favorable for a damage accumulation or a progressive damage approach, since failure is evaluated at each increment. Failure is not evaluated, however, until after equilibrium is reached. This impact is shown in Figure 3.2. As material failure occurs, the stiffness of the material decreases. This change in stiffness can be seen in the figure as the line from point A to point B. The FEM analysis will project along the initial stiffness line to its perceived equilibrium point at C, past the change in stiffness. Then, the failure criterion is implemented and the stiffness terms are reduced.

The FEM response should shift to the actual equilibrium line. This shift will vary depending on the type of input. For load control, the same increment of load will result in a larger displacement, or line CD of the figure. For displacement control, the same increment of displacement will result in a lower value of load, which is line CE of Figure 3.2 . This is known as "load drop" (20).
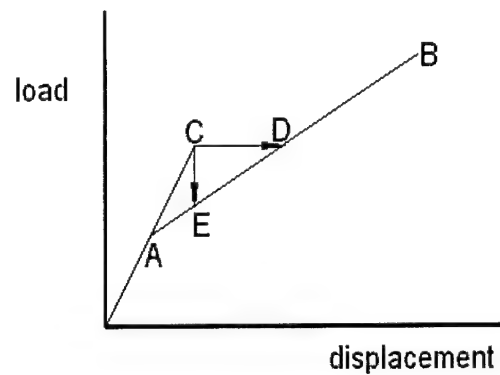

Figure 3.2   Equilibrium Responses to Failure Depending on Type of Input

Once failure occurs, it is preferable to re-apply the same increment to determine the shift to the new equilibrium value, such as from point C to the equilibrium line

in Figure 3.2. If not, it is necessary to use small increments to reduce the amount of error at each determined equilibrium point. This requires many increments, however, which is costly in terms of computational time and negates the benefit of the Newton-Raphson approach. Also, this approach overestimates the final failure value by one step, since another increment is required to produce global structure failure after the "critical" local failure occurs.

Re-applying the same increment once failure occurs is termed "iterating on damage". This requires returning to the previous equilibrium value and projecting forward using the new reduced stiffness matrices. Previous to this research, this capability did not exist in the SLR code. A flow chart of the algorithm for this process is shown in Figure 3.3. Implementing this algorithm requires storing the previous equilibrium position. In the SLR program, this is done through storing the global displacement values at the previous equilibrium point. As the failure criterion is applied, a flag is raised if new failure occurs. This flag tells the code to re-apply the same increment, starting from the previous equilibrium value. The elements are checked for failure and the process repeats until no further damage occurs at that increment. The number of "iterations of damage" depend on the increment size and the size of the element. The program then progresses to the next increment. In this way, the increment that produces global structural failure will be identified. Also, the equilibrium points along the curve will be accurate.

The effect of the progressive failure on an element is shown in Figure 3.4, where failure in an individual element from a $[0/90]_{2s}$ graphite/epoxy panel under tension is plotted as a function of the panel's normalized displacement. The 100% value is the displacement at which the maximum load occurs. An element near the cutout was chosen to demonstrate the failure progression as the damage area grows out from the cutout corner. The failure is broken into matrix and fiber failure in the 0° and 90° plies individually. One-hundred percent failure for a certain ply orientation occurs when all the Gauss points in all those plies exceed the failure criterion. It is noted
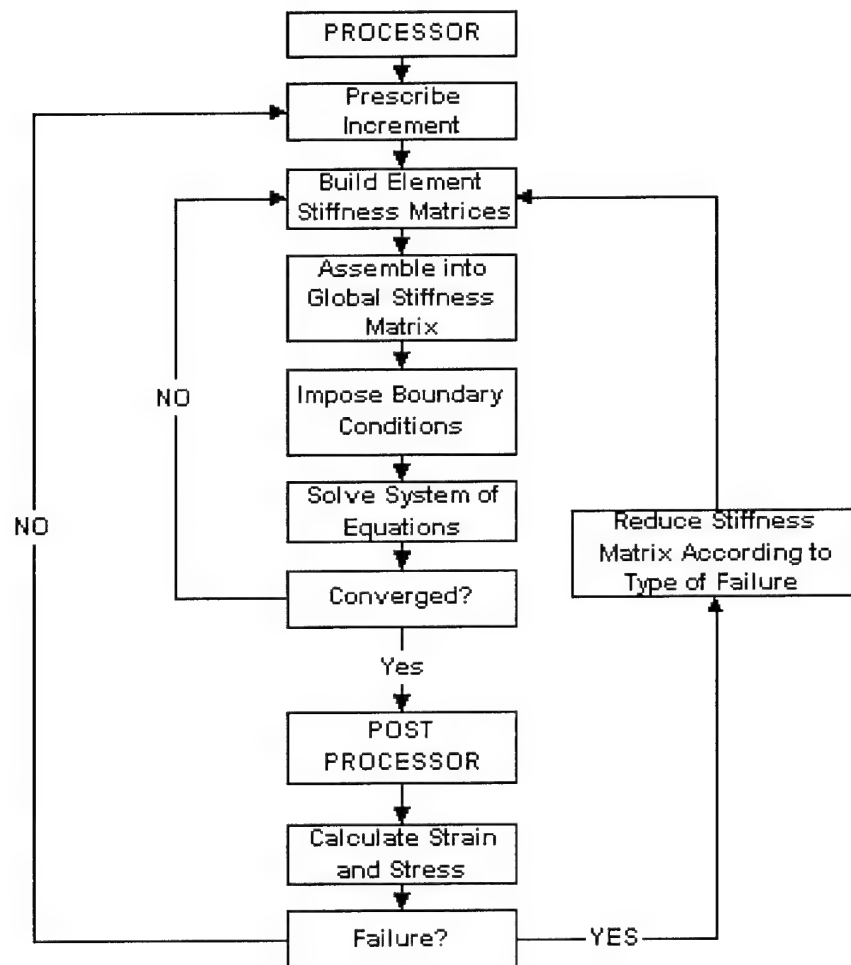
Figure 3.3   SLR Algorithm for Iterating on Damage
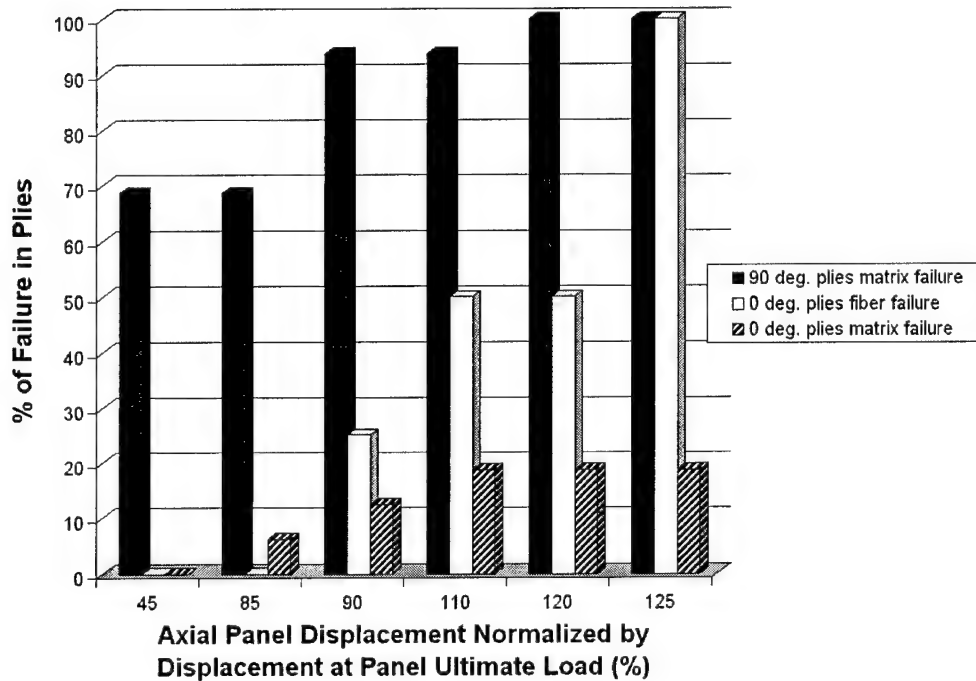
Figure 3.4   Progression of Failure in a Cross-Ply Element under Tension

that fiber failure does not occur in the 90° plies, since the fibers are perpendicular to the primary load. Evidence of the characteristic damage state (CDS) exists in this element at 45% of the ultimate panel value. The 90° plies exhibit 69% failure, which then stabilizes until 90% of the ultimate value, when fibers in the 0° direction fail. Finally, some matrix failure does occur in the 0° plies, but it is obvious from the results that the critical constituent in the 0° direction is the fiber.

3.4   Stiffness Reduction due to Fatigue

The fatigue load is applied at a fraction of the static failure load. If the fatigue value is above the matrix cracking threshold, matrix failure as well as possible localized fiber failure will occur. The new equilibrium value is found and the load is relaxed to its initial value, completing the first cycle. The shell relaxes to a value close to its initial value. There is some slight residual strain, which is acceptable.

Without further adjustments, the shell is in equilibrium. No further failure will be produced for additional cycles between these two load values. Fatigue effects must be accounted for by additional steps. This is done by reducing the material properties, E_1, E_2, G_{12}, G_{13}, and G_{23} for the entire shell. This is a new addition to the SLR code and is performed in the subroutine STRESS at the beginning of each cycle, except for the first cycle. As the program runs through the stress analysis for every element, the properties $Q_{11}, Q_{12}, Q_{22}, G_{12}, G_{13}$, and G_{23} are reduced by a factor (note: Q_{11}, Q_{12}, and Q_{22} are all linear in E_1 and E_2). It is known that stiffness decreases with fatigue, but detailed knowledge of the mechanisms that explain this decrease is not available. Therefore, to account for the stiffness reduction, all properties are reduced equally. This approximation is justified by assuming micromechanical damage occurs in the matrix, the matrix to fiber interface, and possibly even the fiber itself. This is also justified because the code does not accurately account for delamination effects, which can be a fatigue driver in some ply layups (35).

It is not feasible to run the code for 100,000 cycles, as the analysis is time consuming even for a few cycles. Instead, the stiffness reduction factor is scaled to represent a large number of actual fatigue cycles. As seen in Figure 2.5, the secant modulus (stiffness) reduces from approximately 98.5 percent to 97.5 percent in Stage II. This is the region of stable fatigue degradation and the largest portion of life for the composite. In this case, Stage II occurs over 30,000 cycles. To account for this reduction in just a few computational cycles, the material properties, which dictate the overall stiffness, are reduced by a factor, R. Representing the initial stiffness as K_i, the final stiffness as K_f, and the number of computational cycles as n, R can be determined by solving the following equation:

$$K_i R^n = K_f \qquad (3.1)$$

For Stage II:

$$K_i = 0.985K$$

$$K_f = 0.975K$$

$$K = \text{the normalizing (initial) stiffness}$$

Equation (3.1) is now written as:

$$0.985KR^n = 0.975K$$

$$R^n = \frac{0.975}{0.985}$$

$$R = \sqrt[n]{0.98985}$$

For three computational cycles $(n = 3)$:

$$R = 0.9966$$

or $R = 99.66\%$. In this way, one computational cycle represents 10,000 physical cycles. It is now possible to analyze the state of stress and the state of damage of a structure after any number of fatigue cycles by changing the variables n and R.

Without Figure 2.5, a comparison of the initial stiffness and the secant stiffness at failure in the equilibrium curve can be used. This is an approximation, however, because of the development of each stiffness matrix. Remember the stiffness matrix is made up of the individual matrices K, N_1, and N_2, where $N_1 = f(q)$ and $N_2 = f(q^2)$. For the initial stiffness, the displacements q are zero and the N_1 and N_2 matrices are zero. Therefore, there will be difference between the initial and final stiffness values. Both of the above methods are approximations and may not provide the exact results in the number of cycles predicted. Ultimately, the stiffness reduction parameter, R should be varied to whatever value provides the desired results.

The key to accounting for damage progression and fatigue are the two stiffness reduction mechanisms: 1) damage from failure criterion and 2) cyclic loading. Damage from the failure criteria is analogous to macromechanical damage, while it is assumed cyclic loading produces micromechanical damage leading to stiffness reduction. In actuality, macromechanical damage should eventually occur from the individual micro-damage.

3.5 The Finite Element Model

The model chosen for this analysis is a cylindrical panel shown in Figure 3.5. The sides measure 30.48 cm by 30.48 cm [12 in. x 12 in.] and the radius is also 30.48 cm [12 in.]. A 10.16 cm x 10.16 cm [4 in. x 4 in.] cutout is placed in the middle of the panel. This is the same configuration used by Hatfield (6), and allows comparison of compression values with his research. Both cross-ply ($[0/90]_{is}$, where $i = 2$ and 6) and quasi-isotropic ($[0/45/-45/90]_{is}$, where $i = 1$ and 3) configurations are used, resulting in layups of 8 and 24 plies.

3.5.1 Material Properties and Boundary Conditions.

Graphite/epoxy AS4/3501-6 was used for the analysis. The material properties for this composite are shown in Table 3.1 (6), (20):

The boundary conditions were clamped along the top and bottom edges, as this resembles the experimental work of Hatfield. This also models the grips commonly used in experimentation, if further testing is performed for comparison. Even though the ends were clamped, movement in the x-direction only is allowed at one end to apply an axial load or displacement.

For the static analysis, displacement control was used to determine the maximum failure value. The maximum load was determined, and fatigue loads ranging from 30-60% of this value was applied using load control. The main reason for using load control is to apply a constant stress to the shell, which is the conventional S-N
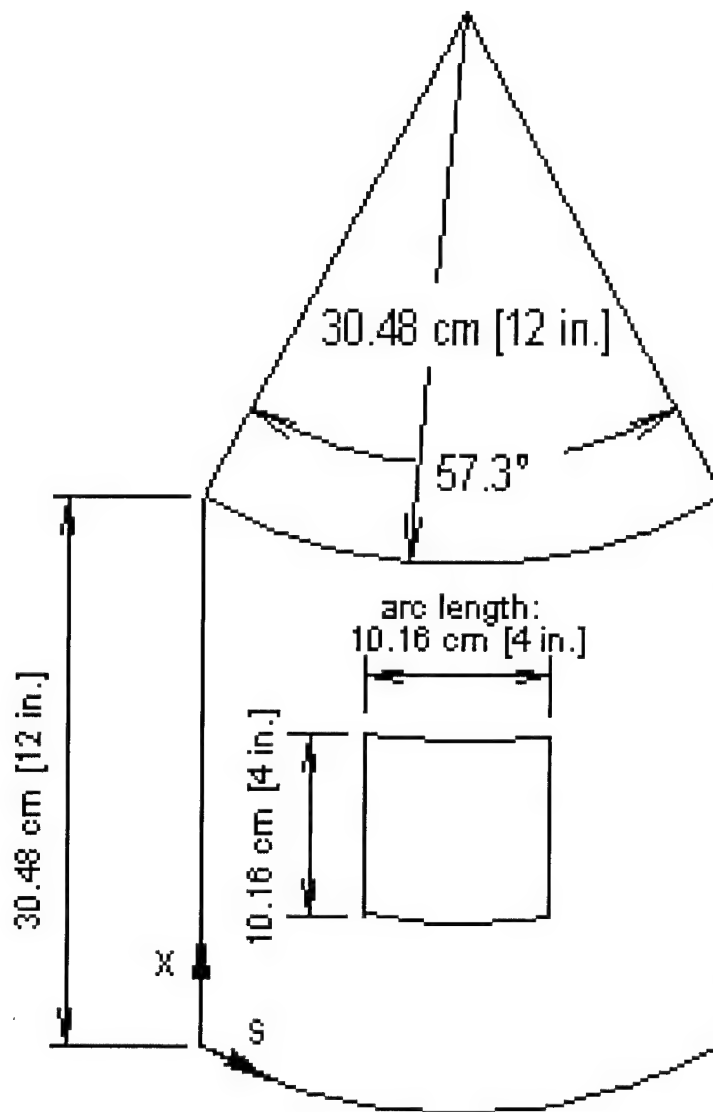
Figure 3.5   Shell Geometry

Table 3.1   AS4/3501-6 Graphite Epoxy Material Properties

Property	SI	English
E_1	135.8 GPa	19.70×10^6 psi
$E_2 = E_3$	10.89 GPa	1.579×10^6 psi
$G_{12} = G_{13}$	6.378 GPa	9.25×10^5 psi
G_{23}	3.185 GPa	4.62×10^5 psi
ν_{12}	0.276	0.276
t_{ply}	0.131 mm	0.00514 in.
σ_{FN}	1.5 GPa	2.176×10^5 psi
σ_{FS}	0.22 GPa	31.91×10^3 psi
σ_{MNT}	43.8 MPa	6.352×10^3 psi
σ_{MNC}	43.8 MPa	6.352×10^3 psi
σ_{MS}	43.8 MPa	6.352×10^3 psi
σ_{DN}	50.0 MPa	7.251×10^3 psi
σ_{DS}	86.0 MPa	12.473×10^3 psi
ϵ_N	0.011	0.011
ϵ_T	0.0065	0.0065

approach. If displacement control were used, the applied stress would decrease as the structure became more flexible due to damage.

For the given configuration, a uniformly applied displacement will not result in a uniformly applied load. This is due to the large cutout, where the structure is more flexible in this region. Therefore, the distributed loads along the edge for displacement control will be the greatest at the ends and the least in the middle. Likewise for load control, a uniform stress distribution along the top edge will result in greater displacements in the middle of the panel, where the cutout reduces the stiffness. An example is shown in Figure 3.6 of the resulting displacement from a uniform applied edge load. Also plotted is the average displacement value. This displacement difference can cause convergence difficulty if this distortion becomes too large.

It is beneficial to note how a uniform stress is distributed to the appropriate nodes in the FEM code for load control. Two possible methods are consistent nodal loads and equivalent nodal loads (41). Equivalent nodal loads is a crude method
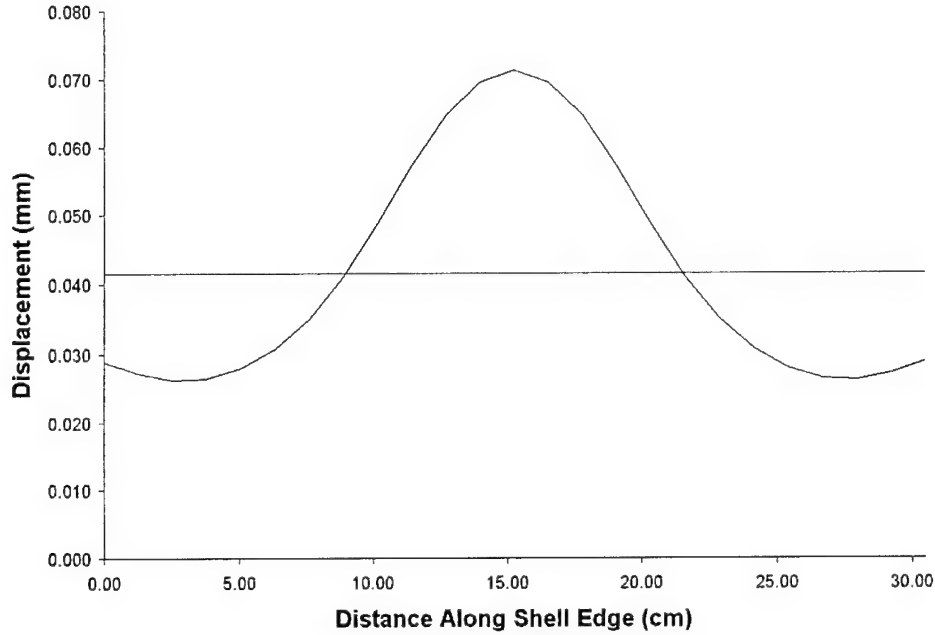
Figure 3.6   Actual and Average Displacement Along an Edge for a Uniformly Applied Stress

where the stress is converted into a force. This force value is then divided by the number of nodes within the application region, resulting in the load being divided equally between all the nodes. There is little or no guarantee that this method will produce a uniform stress field.

For the consistent nodal load method, the degrees of freedom are multiplied by the shape functions. This product is then integrated along the length (for an edge load) to produce the resulting consistent load value at each node (41). For this research, an axially applied load will only vary with the degree of freedom u. The finite element is eight-noded, and the interpolation of u is quadratic. Integrating the quadratic expression for u along an element edge will result in a parabolic representation, with the greatest load being at the mid-side node (41). This parabolic representation has already been programmed into the code. Since the vertex nodes (except for the nodes at each end of the edge) are shared by two elements, their individual load values are summed. This results in a consistent nodal load represen-

3-15

tation for the edge load encountered in this research. This is also true for most of the loading conditions for which the FEM code was designed.

3.5.2 Convergence.
A desirable feature of finite element analysis common to compatible elements, including this element, is that as the number of elements increase, the solution converges to the exact answer. A model with too few elements will present answers more stiff than the actual structure. This is because the model is only allowed to behave according to the interpolation functions chosen (41). To gain precision, either a higher-order interpolation function is required or more elements are needed. However, an increase in the number of elements also increases the complexity and computational time.

For the compression case, the shell fails due to geometric instability. Hatfield (6) used Dennis' (46) findings that an element of the size 1.27 cm x 1.27 cm [0.5 in. x 0.5 in.] provides sufficient accuracy for this type of problem, which is the size element also used for the present compression cases. This results in a 24 element by 24 element array for a panel with no cutout. The interior 8 x 8 elements are removed for the cutout.

To find a balance between convergence and complexity for the tension case, a convergence analysis was performed. An 8-ply, cross-ply configuration was used for the test. The convergence test started with a 6 x 6 array. As mentioned above, displacement control is chosen for the static analysis to determine the maximum point on the equilibrium curve. The number of elements along the edges were doubled until a suitable value was found. The first three arrays are plotted in Figure 3.7. Symmetry was used to increase the number of elements. Symmetry in this manner only applies to the tension loading, since the compression loading fails by geometric instability involving large out of plane displacements. For the current boundary conditions, symmetry exists about the vertical axis as shown in Figure 3.8. Continuity must exist across the arc for symmetry along this vertical axis. Therefore, along the
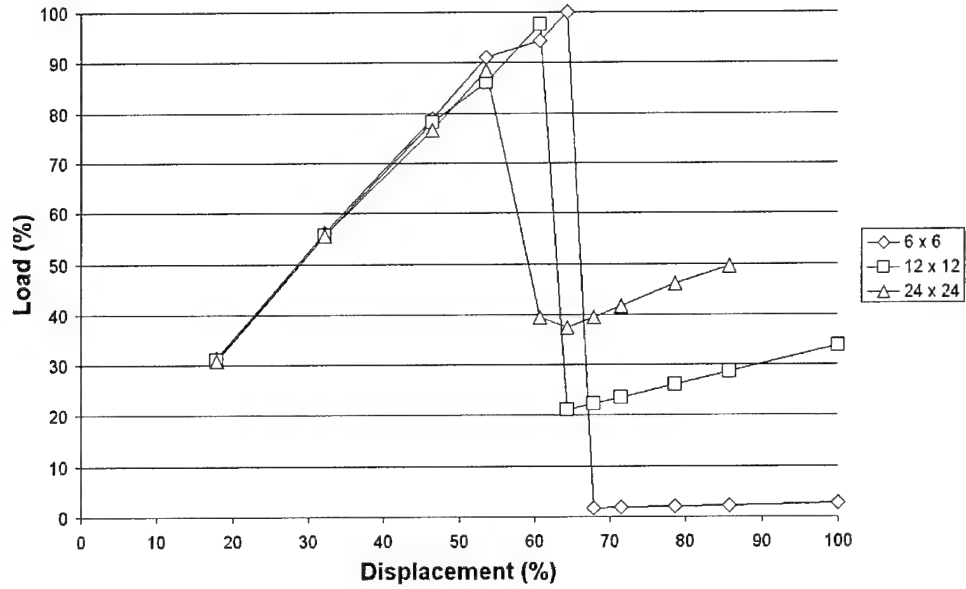
3-16

Figure 3.7   Normalized Equilibrium Curves of Different Size Arrays

vertical symmetry line, the displacement v must equal zero. The slope must also be continuous across this boundary, so $w_{,y} = 0$ is required. By the same token, the rotation Ψ_y must also equal zero.

For symmetry on the horizontal axis, at $x = \frac{L}{2}$, the loading must also be symmetric. Instead of clamping one end and loading the other, it is necessary to load both ends by half the original amount. This results in u being zero at the horizontal symmetry axis, which is required. Continuity also requires that $w_{,x}$, and Ψ_x be equal to zero on this line.

Before implementing quarter-panel symmetric models, it is necessary to validate the above conditions. Analysis of a full 24 element by 24 element panel determines that symmetry does exist. The necessary null degrees of freedom along the respective lines produce values on the order of 10^{-16}, which is assumed a negligible amount. The possibility exists that once failure occurs, this symmetry is lost. However, since the panel exhibits symmetry, the loading and hence the failure ap-
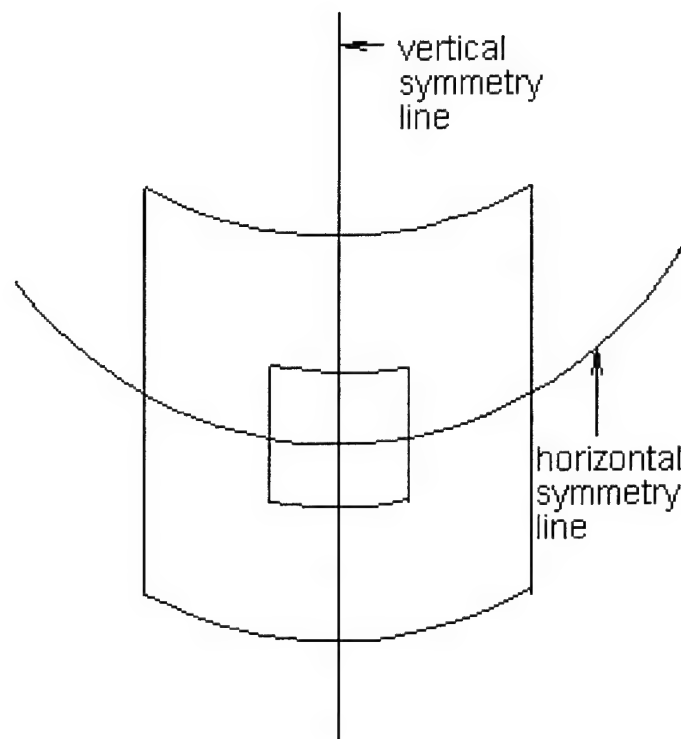
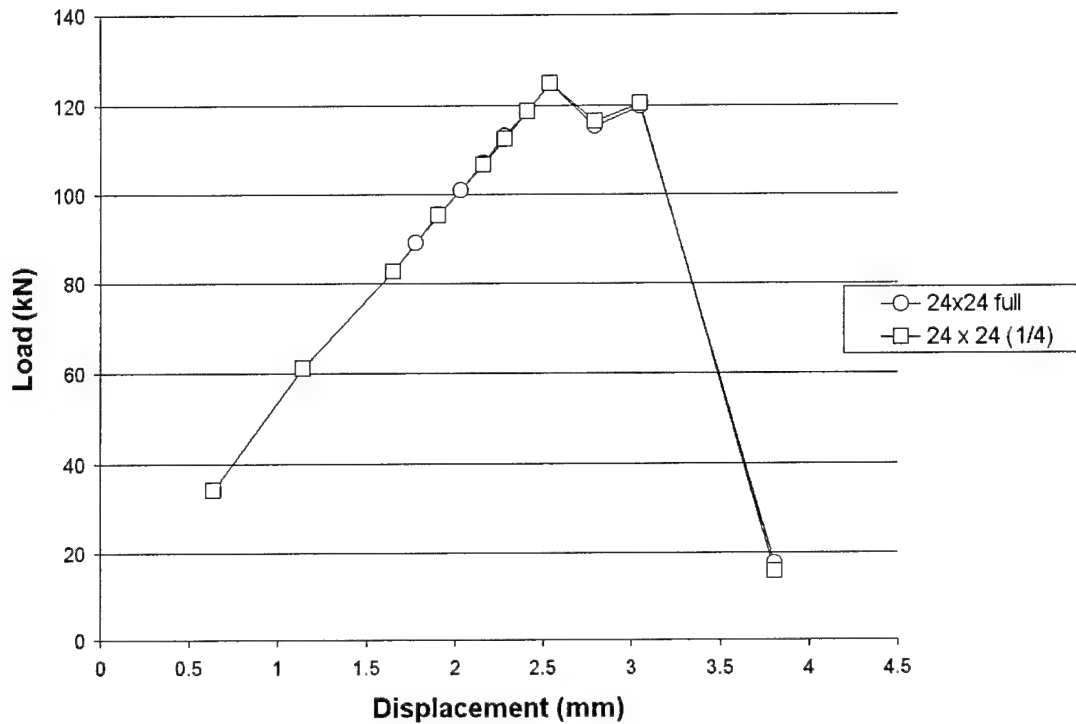Figure 3.8   Shell Symmetry Axes under a Vertical Tension Load

Figure 3.9   Comparison of a Full Panel and a Symmetric Quarter Panel

proximates symmetry or very close to it. Checking the displacement values near failure show that symmetry does begin to break down. Terms that were formerly on the order of 10^{-16} are now on the order of 10^{-4}. These terms are still one to two orders of magnitude smaller than the other displacements, though, and symmetry is still assumed to exist.

Symmetry may be verified by comparing a 24 element by 24 element cross-ply full panel with a symmetrically loaded quarter panel containing the same size elements. The equilibrium curves of both panels is shown in Figure 3.9. In order to perform the quarter panel analysis, the boundary conditions had to be changed. The null degrees of freedom were enforced along the respective symmetry axes, and the appropriate symmetric loading condition was applied to the end. From the figure, it is evident that both panels behave almost identically. Therefore, it is assumed that a full panel may be represented through symmetry by a quarter panel.
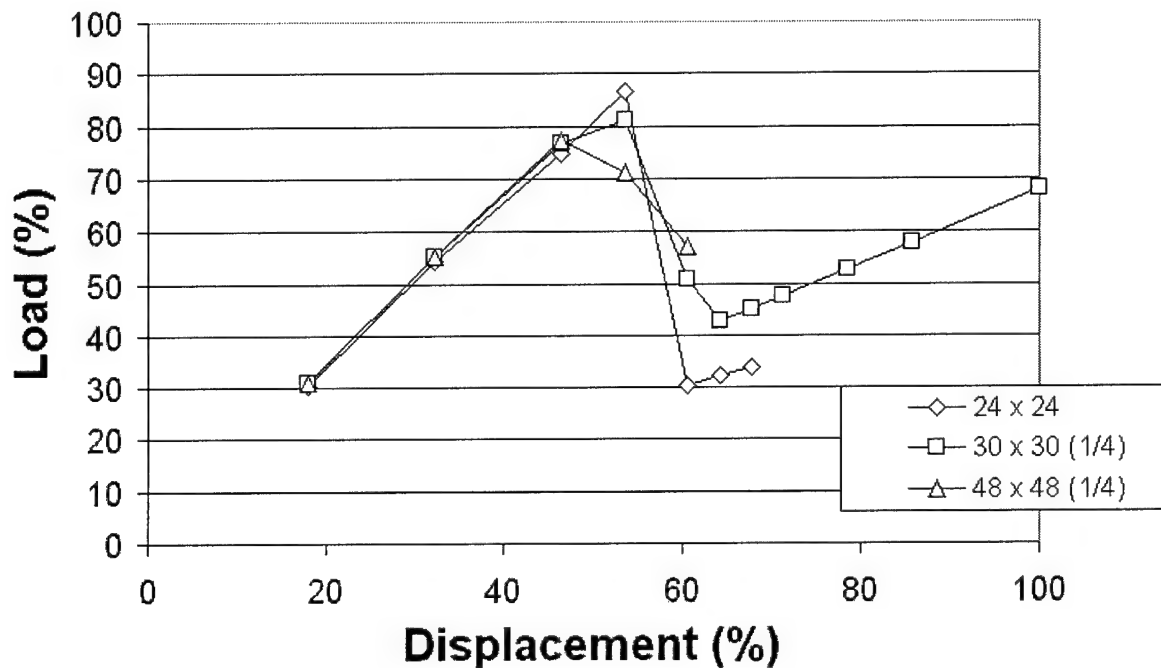
3-19

Figure 3.10   Normalized Equilibrium Curves of More Refined Arrays

It is now possible to continue the convergence check. The number of elements currently allowed by the program (without extensive modification) is 600 elements, which will allow a 24 by 24 element array. A 24 by 24 element symmetric quarter panel models a 48 by 48 element full panel array with an element size of 6.35 mm by 6.35 mm [0.25 in. x 0.25 in.]. Two quarter panel cases were chosen and are plotted in Figure 3.10.

Table 3.2 presents some convergence comparisons. In general, the table and corresponding figures identify the trend that an increase in the number of elements converges toward a less stiff, more exact answer. The ultimate failure value decreases with an increase in the number of elements. There are some anomalies in the chart, however, such as the small reduction in load between the 6 by 6 and the 12 by 12 element arrays. Another is the large reduction is the displacement value at which failure occurs. Therefore, it is advisable to re-evaluate the convergence.

Array Size	Normalized Load (%)	% Reduction	Normalized Displacement (%)	% Reduction
6 x 6	100.0	–	100.0	–
12 x 12	97.6	2.4	94.4	5.6
24 x 24	88.5	9.4	83.3	11.8
30 x 30 ($\frac{1}{4}$ panel)	81.0	6.3	83.3	0.0
48 x 48 ($\frac{1}{4}$ panel)	77.3	4.6	72.2	13.3

Table 3.2   A Comparison of Array Size with Normalized Load and Displacement

Application of the failure criterion plays a crucial role in determining the ultimate panel failure load. In order for the failure criterion to accurately represent the actual material response, there must be an accurate representation of the stress. The cutout is a large stress-riser. From the elasticity approach, the stress approaches infinity near the edge of the cutout. The elements should be small enough to capture an increase in stress near the cutout. To analyze this, a local convergence test is performed. The stress along a ray from the corner of the panel to the corner of the cutout is plotted. This is performed for the various array sizes and is shown in Figure 3.11.

A singularity does exist at the sharp cutout corner, however, and the assumptions made for the finite element analysis begin to break down. Again, FEM must meet the necessary requirements on an average sense, and not necessarily at each element. Therefore, stresses in the element adjacent to the cutout will be in error. In fact, a large element adjacent to the cutout will "smear out" some of the effect of the singularity and its resulting inequality. A balance between element size is preferred.

From Figure 3.11, it is observed that the 6 x 6 and 12 x 12 arrays actually decrease in stress near the cutout. Clearly, elements of this size are too crude. The 48 x 48 element array displays a large increase in stress near the cutout corner. At a distance of about 1.5 cm [0.6 in.] away from the cutout corner, however, the 48 x 48, 30 x 30, and 24 x 24 element arrays represent approximately the same stress value.

From this comparison, it is observed the failure criteria will be more effective if smaller elements are used. As the element size decreases, a higher change in stress can be detected—resulting in failure at a lower global input value. It is this failure that is driving down the displacement at which ultimate failure occurs from the previous figures. For most composite configurations, the fiber is the "critical element" (28). The residual strength of the composite relies on this critical element. Having fibers fail at a lower load—even in a smaller element—causes further element and eventually ultimate panel failure at a lower load and displacement value. Therefore, a model with smaller elements does a better job of approximating an actual structure.

The argument against smaller elements is computer run-time. Even using "banded" matrices, computer runs take a long time due to the nonlinear nature of the analysis and the amount of information that must be generated. For a 6 x 6 element array, one increment often takes 10 minutes on a Spark 20 Sun Workstation. If failure occurs, this increment must be re-applied. For a 24 x 24 array, a problem using failure criteria and involving 10 increments often takes 120 hours or more to complete. In developing the technique of handling fatigue failure, it is deemed necessary to reduce the size of the model if possible. A 12 x 12 array has a run-time of approximately 24-36 hours. Using symmetry and a 1.27 cm x 1.27 cm [0.5 in. x 0.5 in.] size element is a good balance between accuracy and efficiency. It should be sufficient to identify trends in the analysis in a reasonable amount of time.
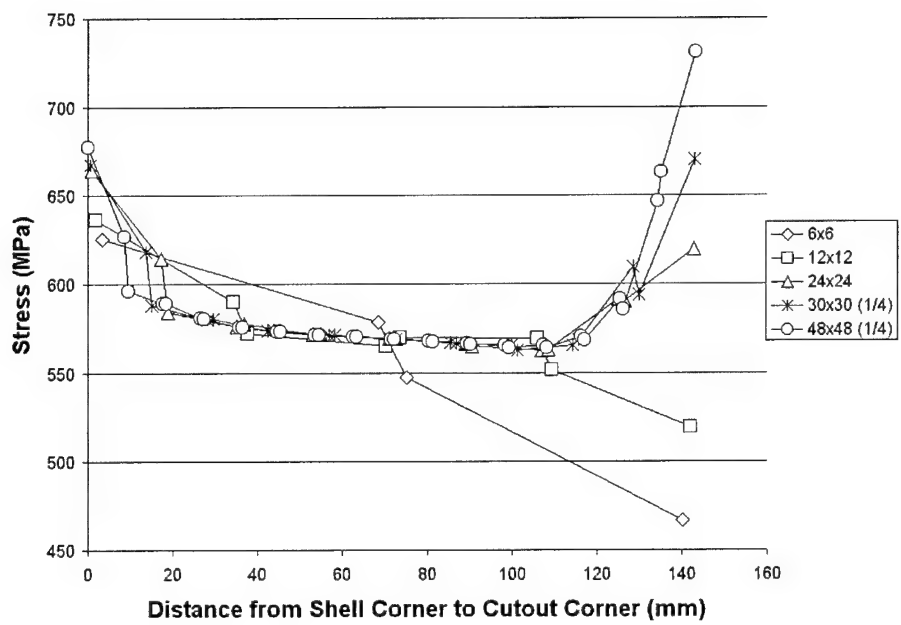
Figure 3.11   Stress Distribution for Various Array Sizes

IV. Results and Discussion

4.1 Shell Static Failure

Before the fatigue results are analyzed, it is important to observe the results of the static loads. These will identify trends in the panel behavior as well as establish parameters for the fatigue loading.

4.1.1 Static Compression.

In compression, the shell fails from instability, or collapse. In this failure mode, the shell deflects axially until it is no longer able to store the applied energy. Then, a large out-of-plane deflection results from the axially applied load. It is determined that very little material failure occurs, although there is some localized matrix failure due to compression. This material failure does little to change the panel's ultimate collapse load. Comparison with Hatfield's (6) computational results in Table 4.1 shows a 7.5% reduction in collapse load, but is still 14 % above the experimental results for the $[0/90]_{2s}$ configuration. Also, the displacement at collapse has a slight but negative change from computational results that do not consider material failure. The quasi-isotropic ply yields similar results.

Table 4.1   The Effect of Material Failure in Collapse Analysis

Type	Collapse Load (N) [lbs]	Displacement at Collapse (mm) [in.]
Cross-ply with Material Failure	5,831 [1,311]	0.25 [0.010]
Cross-ply without Material Failure (6)	6,307 [1,418]	0.28 [0.011]
Cross-ply Experimental Results (6)	5,115 [1,150]	1.02 [0.040]
Quasi-isotropic with Material Failure	5,747 [1,292]	0.22 [0.009]
Quasi-isotropic without Material Failure (6)	6,272 [1,410]	0.25 [0.010]
Quasi-isotropic Experimental Results (6)	4,403 [990]	0.711 [0.028]

4.1.2 Static Tension.

Material failure is the primary cause of panel failure for the tension case. This is displayed through the determination of
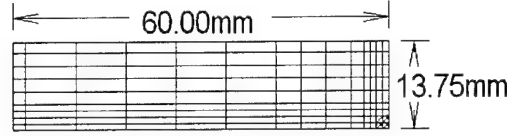
60.00mm

13.75mm

Figure 4.1   FEM Model of Plate used for Comparison with Jen, et al.

Configuration	Jen, et al. (MPa) [ksi]	FEM Analysis (MPa) [ksi]	% Difference
$[90/0]_{4s}$	258 [37.4]	260 [37.7]	0.8
$[\pm 45]_{4s}$	73 [10.6]	106 [15.4]	45.4
$[0/90/\pm 45]_{2s}$	203 [29.4]	225 [32.6]	10.8
$[90/0/\pm 45]_{2s}$	141 [20.4]	225 [32.6]	59.6

Table 4.2   Comparison of Results for Flat Plate with a Hole

ultimate load, displacement at ultimate load, and failure progression through the panel for the static case.

In order to validate the approach, comparison is made with experimental results. Results for the curved shell in tension were not available, so comparison is made with experimental results for a flat plate from Jen, et al. (34). A 12.0 cm x 2.75 cm [4.72 in. x 1.08 in.] plate with a 0.4 cm [0.16 in.] diameter hole was compared for 4 different configurations. Symmetry was used to develop a quarter-plate FEM model, which is shown in Figure 4.1. The comparisons are in Table 4.2.

The $[90/0]_{4s}$ configuration is extremely close to the actual value, and this develops confidence in the ability of the Hashin failure criteria to capture the damage within the plate. There is a much larger variance in the results for the $[+45/-45]_{4s}$ and $[90/0/\pm 45]_{2s}$ configurations. This is because delamination plays a larger role in the failure of these configurations. As mentioned in Chapter 3, the current approach does not capture delamination failure well.

Just by varying the ply layups in the quasi-isotropic configurations causes an increase in delamination initiation. Jen (34) states that delamination begins for the

Table 4.3   Static Analysis Results for 8-ply Graphite/Epoxy under Axial Tension

Configuration	Ultimate Load (N) [lbs]	Displacement at Ultimate Load (mm) [in.]
Cross-ply	124,958 [28,092]	2.54 [0.10]
Quasi-isotropic	99,645 [22,401]	3.048 [0.12]

$[0/90/ \pm 45]_{2s}$ case between the 0° and 90° plies, but almost at the panel ultimate stress. For the $[90/0/\pm45]_{2s}$ case, delamination begins between the 0° and +45° plies. This is because the 0° ply is the primary axial load carrying ply. Having the +45° ply adjacent to this ply causes a large shear stress between the two plies, resulting in delamination initiation at a lower stress. For cases where delamination is not the primary failure mode of the composite, the FEM code with the Hashin criterion does a good job of modeling the failure progression and capturing the ultimate stress.

An 8-ply cross-ply ($[0/90]_{2s}$) and a quasi-isotropic ($[0/ \pm 45/90]_s$) shell were analyzed quasi-statically until failure. Displacement control was used to determine the panel ultimate load value, and the results are listed in Table 4.3. The equilibrium curves for these configurations are shown in Figure 4.2.

The progression of failure through a cross-ply panel is plotted in Figures 4.3 and 4.4. For certain points along the equilibrium curves shown in Figure 4.2, a "snapshot" of failure is taken. The data shows that membrane stresses dominate over bending stresses in tension loading in the panel. That is to say, for a certain ply orientation the stress is approximately uniform through the thickness. Failure is not distinguished for individual plies, but plies of one orientation tend to show the same amount of failure. Therefore, if matrix failure occurs in a 90° ply, it often occurs in every 90° ply. The same applies to fiber failure in the 0° plies. There are a few exceptions to this, but they are usually localized and away from the progressing damage front. Also, failure is determined to exist in the ply if at least 50% of the Gauss points within that ply have failed.
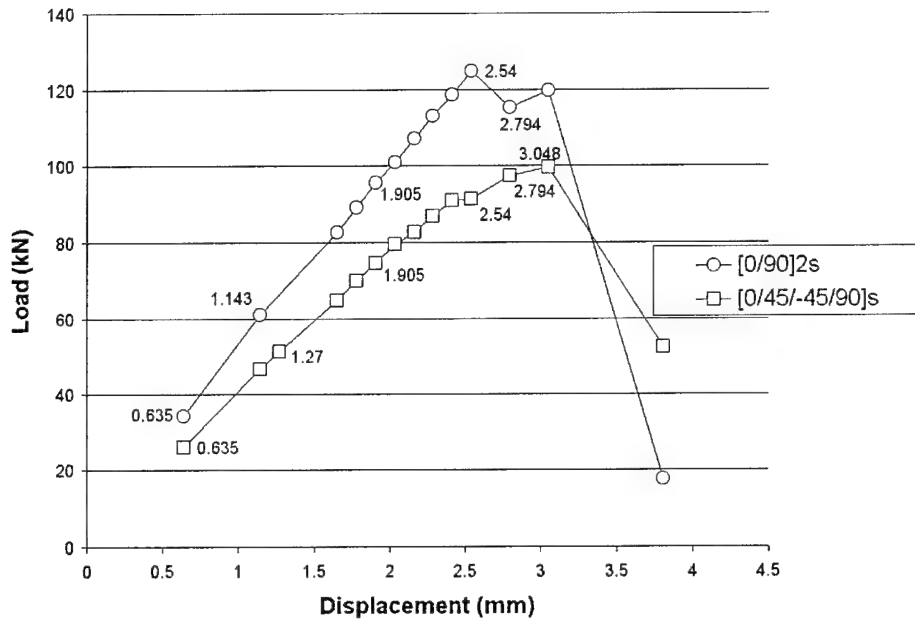
Figure 4.2   Equilibrium Curves for Two Laminates under Axial Tension

Failure in the 0° plies is plotted in Figure 4.3. The primary failure mode is fiber failure, but the matrix may also fail due to tension in these plies. Figure (a) shows that first fiber failure occurs near the cutout as expected, and at a very high load. Fiber failure extends vertically along the edge of the cutout, as well as progressing across the width in (b), which is perpendicular to the primary load direction. Also notice some matrix failure due to compression occurs along the "hidden" edge of the cutout. Figure (b) is at the panel's ultimate or maximum load. As shown in figures (c) and (d), just a small increase in displacement causes the damage front to progress across the panel, leading to panel failure.

For the 90° plies, failure is already evident at a displacement of 0.635 mm [0.025 in.], corresponding to an axially applied load of 34.2 kN [7,683 lbs.]. As shown in Figure 4.4(a), this is a matrix failure due to tension. Once the displacement reaches 1.143 mm [0.045 in.], the characteristic damage state (CDS) has occurred, as shown in (b). Matrix cracking has occurred and stabilized in the panel. A further increase

in applied displacement only results in a few more matrix failures for the 90° plies, as seen in figure (c).

As mentioned in Chapter 1, there are different approaches to analyzing failure in a composite. One approach is the fracture mechanics approach, which bases failure on a crack type of damage. While Figure 4.3 does shown a crack-like damage progression, the damage occurs over the width of several elements. This leads to another approach for failure, the damage growth method. Because of the different constituents and orientations in composite laminates, failure is often spread across an area. This is especially obvious for the 90° ply failures in Figure 4.4. While this is not the primary damage leading to panel failure, the combination of the fiber and matrix failures over several elements validates use of a damage area or accumulation approach.

Similar results are plotted for a quasi-isotropic 8-ply shell in Figures 4.5 - 4.8. From these figures, it is seen that the damage pattern takes a different shape. This configuration lends itself well to the damage progression failure model. Again, failure originates in the 90° plies near the cutout. The −45° plies are the next to show large-scale failure. These plies are adjacent to the 90° plies, and must pick up the stress distribution due to the early 90° ply matrix failure. The +45° plies fail in matrix next, and finally, the fibers in the 0° plies fail. The failure pattern spreads out in a 45° pattern, including the fiber failures. In general, this damage pattern correlates with experimental failure patterns, such as that found in Daniels, et al. (47).

It is important to note that in both configurations, delamination was not shown to occur. According to Barboni et al.(35), delamination is not very prevalent in cross-ply laminates. However, delamination did not occur for the quasi-isotropic panel either, nor after a large amount of failure occurred in either the panel. This departs from the common knowledge that delamination is an active damage mechanism in laminate composites.
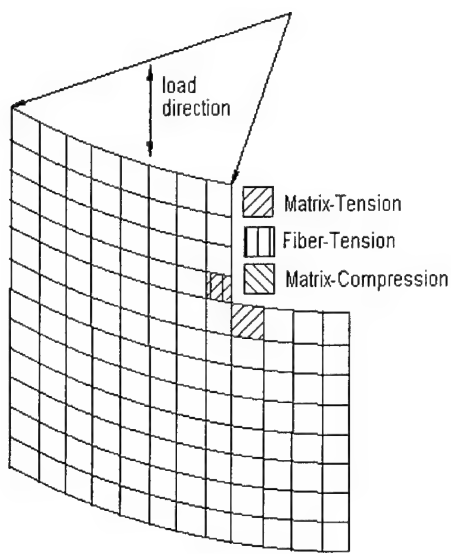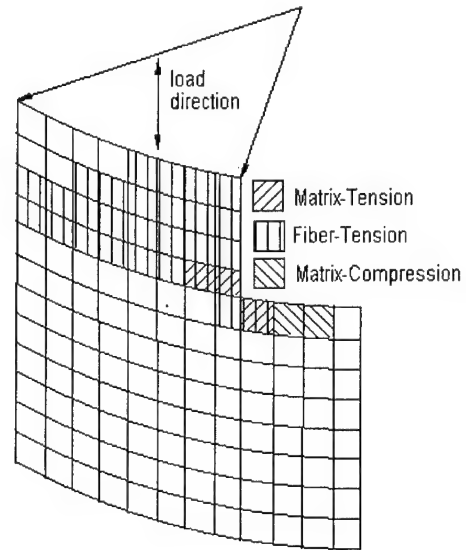
(a) Displ.=1.905mm, Load=95.5kN
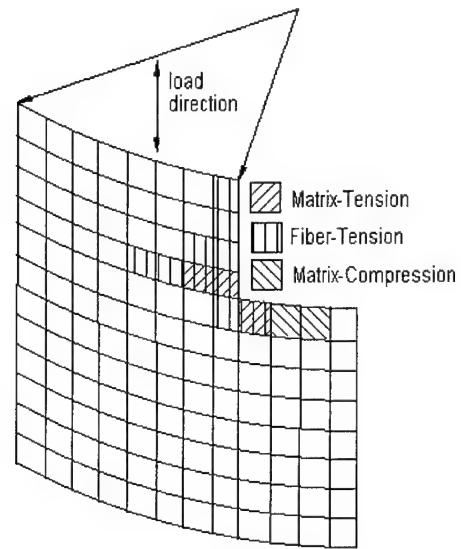
(b) Displ.=2.54mm, Load=125.0kN
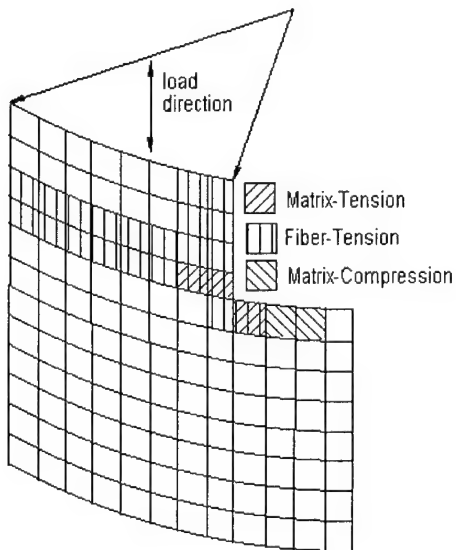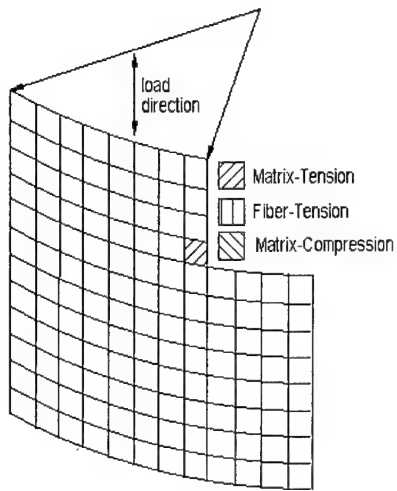
(c) Displ.=2.794mm, Load=115.3kN

(d) Displ.=3.048mm, Load=119.7kN

Figure 4.3   Failure Progression for 0° Plies in a Cross-ply Shell

(a) Displ.=0.635mm, Load=34.2kN

(b) Displ.=1.143mm, Load=61.0kN
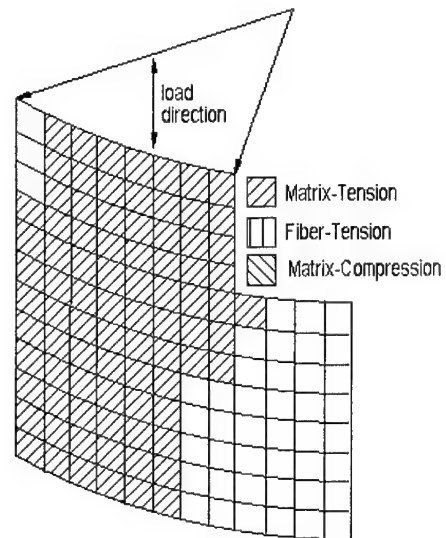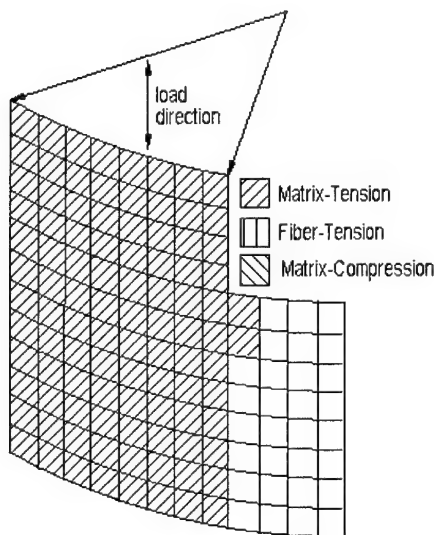
(c) Displ.=1.905mm, Load=95.5kN

Figure 4.4   Failure Progression for 90° Plies in a Cross-ply Shell
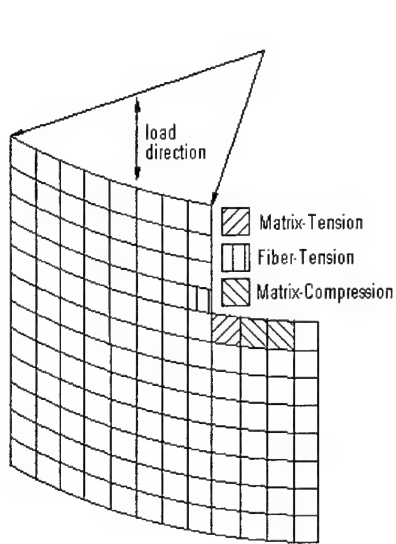
(a) Displ.=1.905mm, Load=74.7kN

(b) Displ.=2.54mm, Load=91.4kN
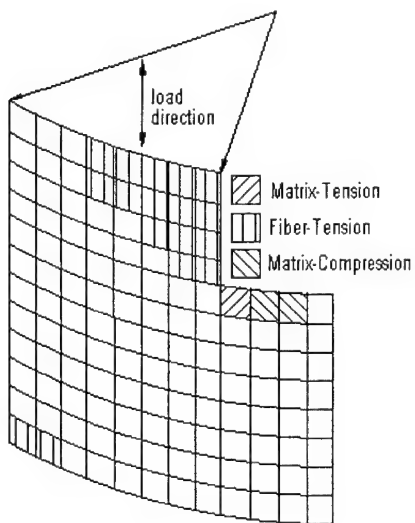
(c) Displ.=2.79mm, Load=97.3kN

(d) Displ.=3.048mm, Load=99.6kN

Figure 4.5   Failure Progression for 0° Plies in a Quasi-Isotropic Shell

(a) Displ.=1.27mm, Load=51.4kN
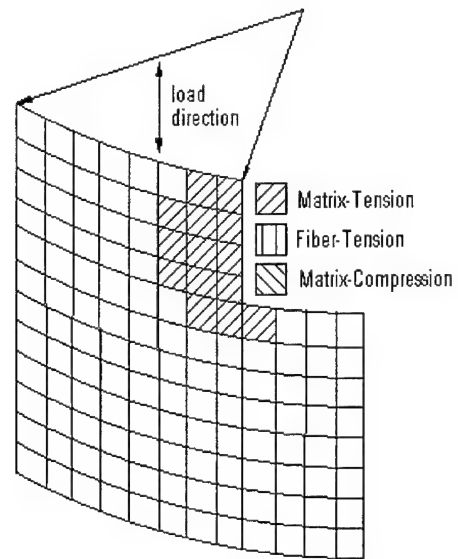
(b) Displ.=1.905mm, Load=74.7kN
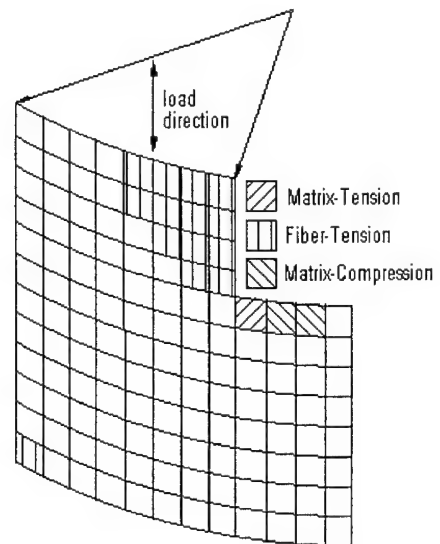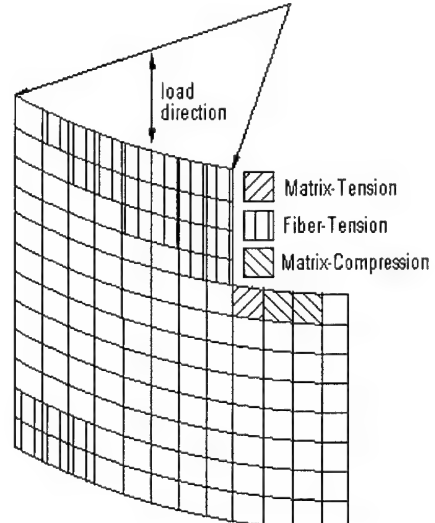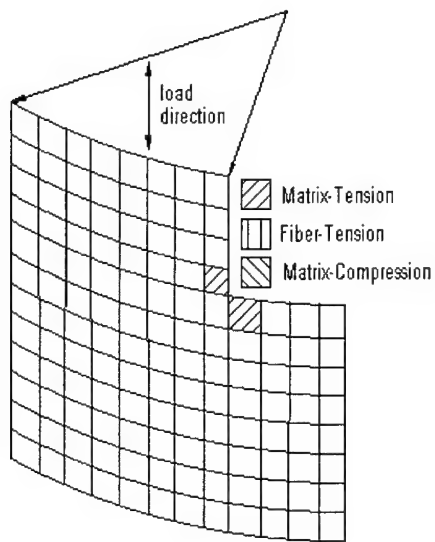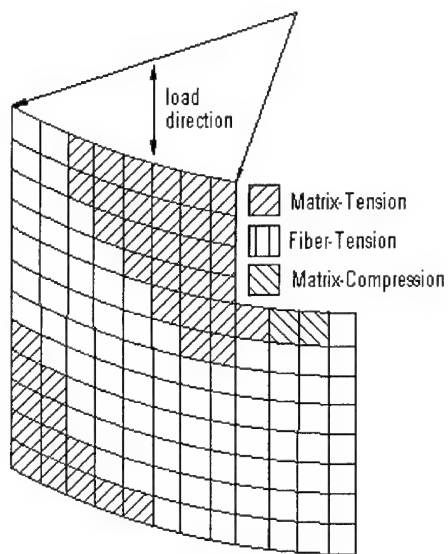
(c) Displ.=2.54mm, Load=91.4kN
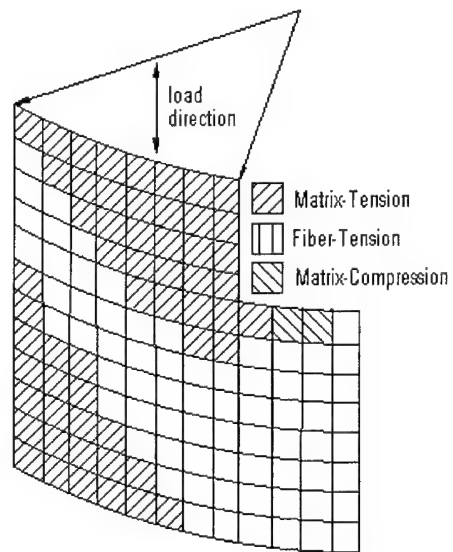
(d) Displ.=2.79mm, Load=97.3kN

Figure 4.6   Failure Progression for +45° Plies in a Quasi-Isotropic Shell

(a) Displ.=1.905mm, Load=74.7kN

(b) Displ.=2.54mm, Load=91.4kN
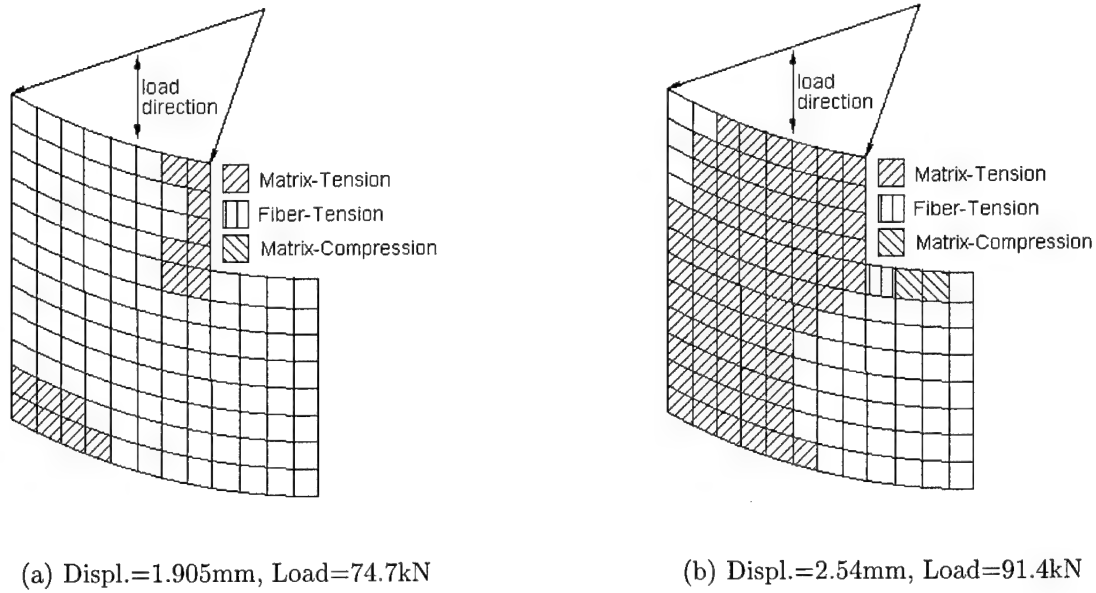
Figure 4.7   Failure Progression for $-45°$ Plies in a Quasi-Isotropic Shell

There are several reasons why delamination did not appear in the results, which have been mentioned previously. From the chosen delamination failure criterion, the stresses contributing to delamination are σ_{33}, σ_{23}, and σ_{13}. Again, σ_{33} is assumed to be zero by the theory. Therefore, only σ_{23} and σ_{13} (σ_4 and σ_5 in our notation) are capable of causing delamination. If free-edge effects were considered, these stresses would increase near the boundaries. Free-edge effects are not considered in the theory, so this increased stress distribution due to the free-edge is not captured. Lee (18) also encountered this problem with the criterion he developed, stating an inability to refine the mesh near the edge to capture these effects.

4.2   Shell Fatigue Loading

Load control is used in order to apply a constant stress. After the first cycle, the stiffness is arbitrarily reduced to model experimental fatigue results. Load control results in an uneven displacement along the edge where it is applied. This is due to the reduced panel stiffness in the area of the cutout. In order to plot the equilib-
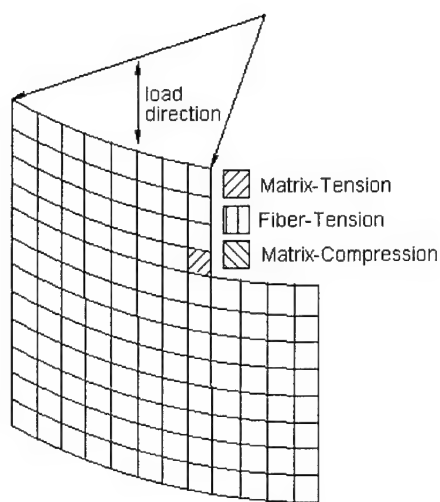
(a) Displ.=0.635mm, Load=25.9kN
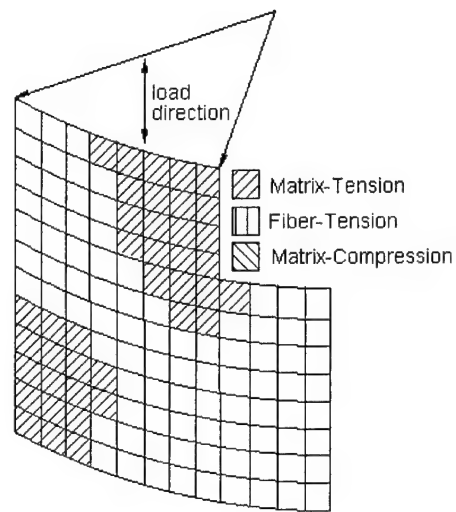
(b) Displ.=1.27mm, Load=51.4kN
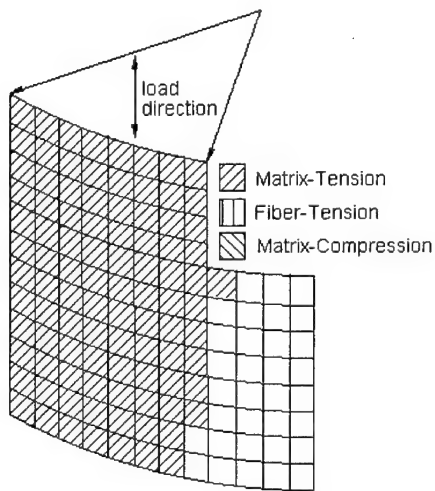
(c) Displ.=1.905mm, Load=74.7kN

Figure 4.8   Failure Progression for 90° Plies in a Quasi-Isotropic Shell

rium curve, the average displacement across the edge is used. Several combinations of load value, stiffness reduction parameter, number of cycles, and ply thicknesses were evaluated. This is a benefit of this approach, since the parameters may be adjusted to highlight certain effects. Due to similarity, only the results for the 8-ply

Table 4.4   Fatigue Parameters for the Compression Equilibrium Curves

Configuration	Fatigue Load as % of Collapse Load	Stiffness Reduction Parameter, R	Number of Computer Cycles Applied
Cross-ply	29	0.90	6
Quasi-isotropic	29	0.995	6

configurations are shown—for both the cross-ply and the quasi-isotropic cases. Equilibrium curves for compression and tension are plotted for a representative model for each configuration.

4.2.1 Compression.   In compression, panel failure is mainly due to geometric nonlinearities and not material failure. The compression loadings in fatigue were very sensitive to the fatigue stiffness reduction parameter, R. If R were too large, the FEM code would not converge, even on the first fatigue cycle. If it were too small, final panel failure due to fatigue would not occur. Table 4.4 lists the fatigue parameters for the configurations corresponding with the displayed equilibrium curves.

The effects of the stiffness reduction can be seen in the increase in axial displacement that occurs each computer cycle in Figures 4.9 and 4.10. It is important to remember that one computer cycle represents thousands of actual fatigue loading cycles. For the cross-ply panel, the larger change in stiffness each cycle shows a large change in axial displacement. The stiffness reduction for this chart is 0.90. The maximum axial displacement reached is 0.082 mm [0.003 in.]. The displacement at collapse for this panel is 0.25 mm [0.009 in.], so many more cycles are required before collapse occurs by fatigue for this applied load. Comparing the change in stiffness values each cycle shows a 90% reduction, which correlates exactly with the stiffness reduction parameter. Since the reduction parameter, R, is 0.995 for the quasi-isotropic panel, there is very little change in displacement each cycle.

After these runs, the conditions were changed to show final collapse in fatigue. This was achieved in four cycles for both configuration at a fatigue load 60% of the

4-12
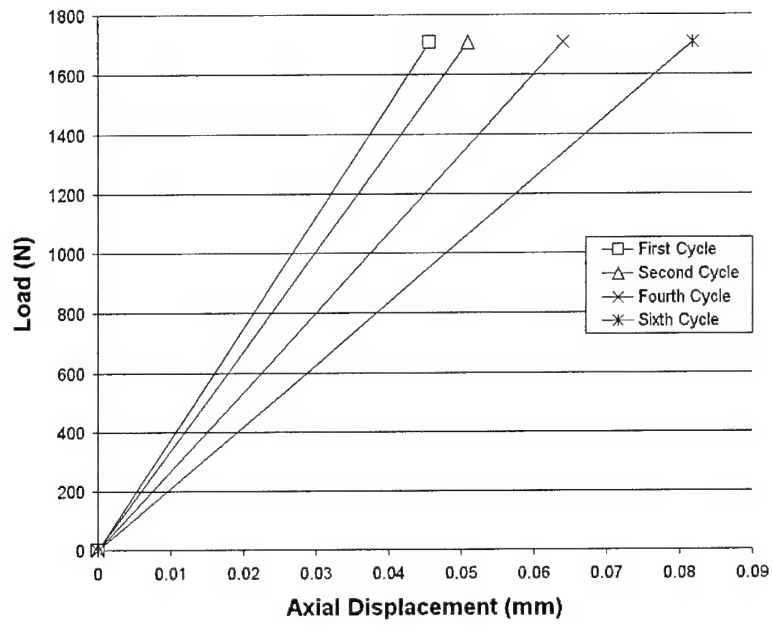
Figure 4.9   Fatigue-Compression Cycles for a Cross-ply Shell-(29% Load)
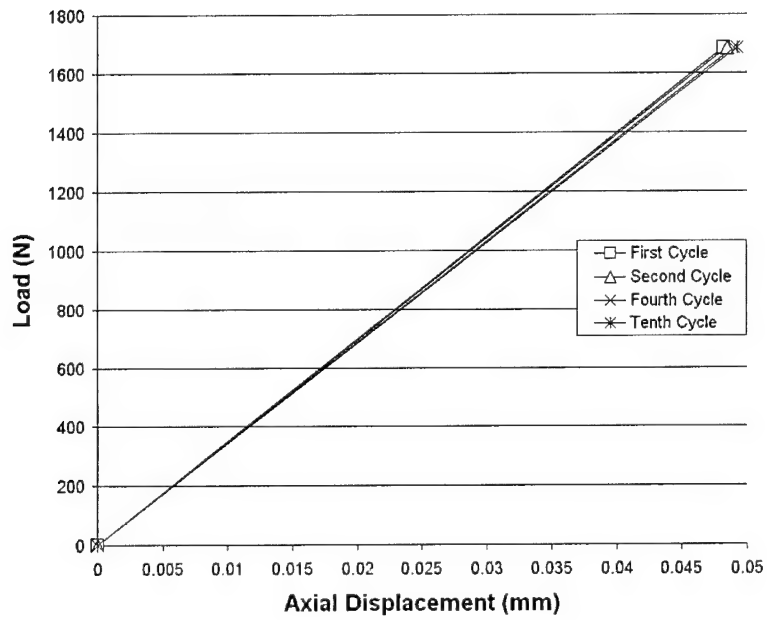
Figure 4.10   Fatigue-Compression Cycles for a Quasi-isotropic Shell-(29% Load)
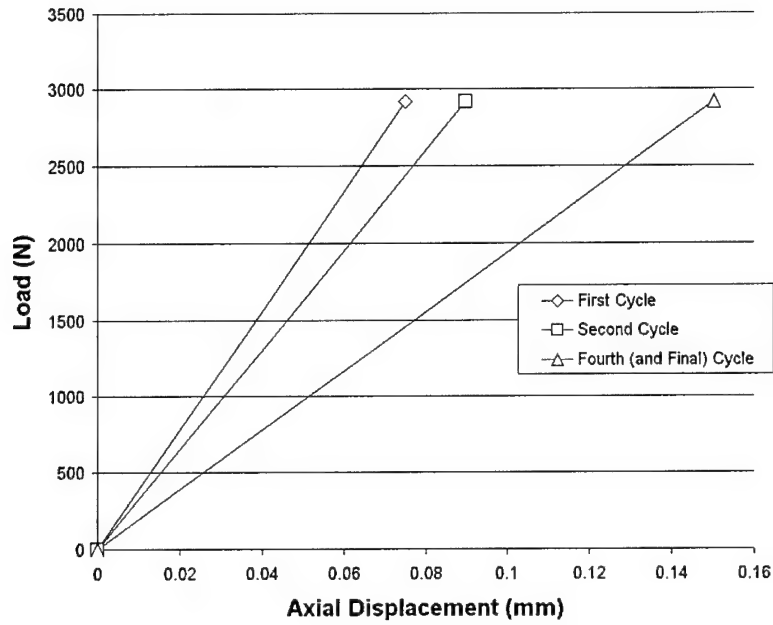
Figure 4.11   Fatigue-Compression Cycles for a Cross-ply Shell-(60% Load)

collapse load and an R of 0.88. For the cross-ply configuration, the displacement at collapse is 0.15 mm, shown in Figure 4.11. This is much lower than the quasi-static results for displacement at collapse, which was 0.25 mm. The same effect occurred for the quasi-isotropic panel, so those results are not shown. The fatigue collapse displacement was at 0.17 mm, compared to the static collapse displacement of 0.22 mm.

4.2.2   Tension.   In tension, the individual failures cause a change in slope in the equilibrium curve. This material nonlinearity can be accounted for by applying the failure criterion and iterating until the new equilibrium value is reached. To account for the stiffness reduction due to fatigue, the stiffness terms are reduced by a set amount each cycle. Again, several configurations and parameter values are used, and the results for the 8-ply cross-ply and quasi-isotropic panels are displayed to show the trends. The fatigue parameters for the displayed configurations are listed in Table 4.5.

Table 4.5 Fatigue Parameters for the Tension Equilibrium Curves

Configuration	Fatigue Load as % of Ultimate Load	Stiffness Reduction Parameter, R	Number of Computer Cycles Applied
Cross-ply	30	0.88	11
Quasi-isotropic	32	0.88	11

Figures 4.12 and 4.13 display the different equilibrium curves for the tension case. Again, cycle is referring to a computer load cycle which represents thousands of actual fatigue cycles. From these curves, it is observed that panel failure is never reached. Even though the applied load is low (30% of ultimate), it is high enough to generate localized failure near the cutout for the first cycle. If a higher load were applied, or a larger stiffness reduction introduced, panel failure would occur. For example, the stiffness reduction parameter, R, for the cross-ply panel was reduced to 0.60, and panel failure occurred in four computer cycles. Since load control is employed, panel failure results in either the convergence criteria being exceeded or a sudden occurrence of a very large displacement. This is because the load control method cannot traverse the maximum point on the equilibrium curve.

Another interesting effect of the fatigue stiffness reduction technique for tension loading is that no further material failure occurs. From before, $F = kd$ or $R = Kq$. Since R is applied at the same value and K is reduced, q increases. The stress in the load carrying elements remains approximately the same. Therefore, this technique will never generate macromechanical critical failure for a stress-based failure criterion. An interesting result does occur, however. In the "hidden" region below the cutout, no global tension load is carried. The load at this point has "sheared" out around the cutout. In fact, results from the static test show compression in this area. For the analysis, the only material failure with the Hashin criterion for the panel due to fatigue is in this area. The panel's global displacement is causing an increased compressive stress in this local region, which results in matrix compressive failure. This region is not the primary load-carrying region, however, and it does not affect the panel's ultimate response.

4-15
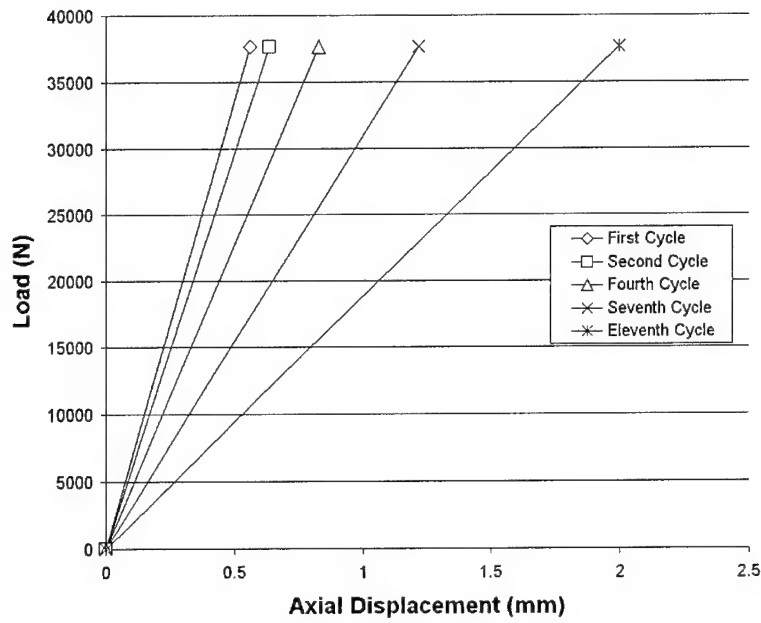
Figure 4.12   Equilibrium Curves for a Cross-ply under Tension-Fatigue
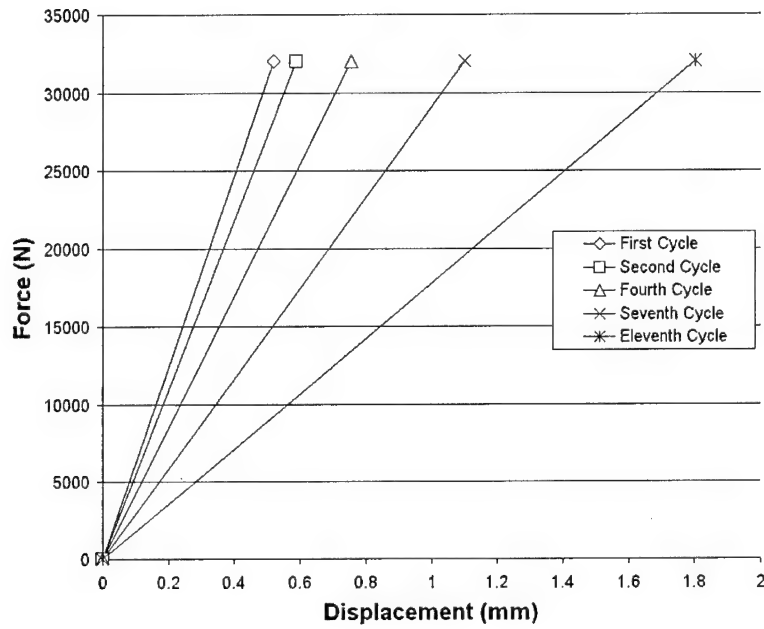
Figure 4.13   Equilibrium Curves for a Quasi-isotropic Panel under Tension-Fatigue

4-16

Since the displacement and strains are increasing in each element, but not the stress, a strain-based failure criterion was added. The maximum strain failure criterion was used to account for the macro-damage that leads to the end of the fatigue life. The first cycle is applied as before, and the Hashin failure criterion is used. The new equilibrium point is determined from this failure, and then the load is relaxed. The maximum strain criterion is then applied on the next cycle. To avoid redundancy, the strain criterion is not applied to Gauss points which have already failed (by the Hashin criterion).

The 8-ply cross-ply configuration was used to test the addition of the maximum strain failure criterion. The equilibrium curves are shown in Figure 4.14. For this case, the stiffness reduction ratio, R, was kept at 0.88, and the load was 30% of the ultimate panel load. With the maximum strain criterion, panel failure occurred in five cycles. Therefore, this technique is able to model all three phases of the fatigue life in the axial tension case. As determined before, the panel cannot withstand much fiber failure. Fiber failure in strain occurs in the fifth cycle. This failure originates at the element adjacent to the cutout, just as it did in the static case. Further element failure in this cycle propagates out from this element, resulting in element failure from both the Hashin and strain criteria. In this way, the maximum strain criterion is a "catalyst" to start the final fatigue failure present in Stage III.

Reducing the stiffness of the panel simulates the affect of fatigue. The stress distribution during the fatigue cycle, after CDS, is determined, as well as the panel displacement values. In the fatigue cycles, the displacements and strains are provided at virtually any location. For the compressive fatigue loads, where the mode of failure is primarily due to geometric instability, no additional failure criteria are needed. For the tension fatigue loads, where material failure dominates the ultimate failure mode, the maximum strain criterion is used to initiate failure in the critical constituent— which is the 0° fibers near the cutout. This technique is now able to capture all three stages in the life of a composite material for either compression or tension.
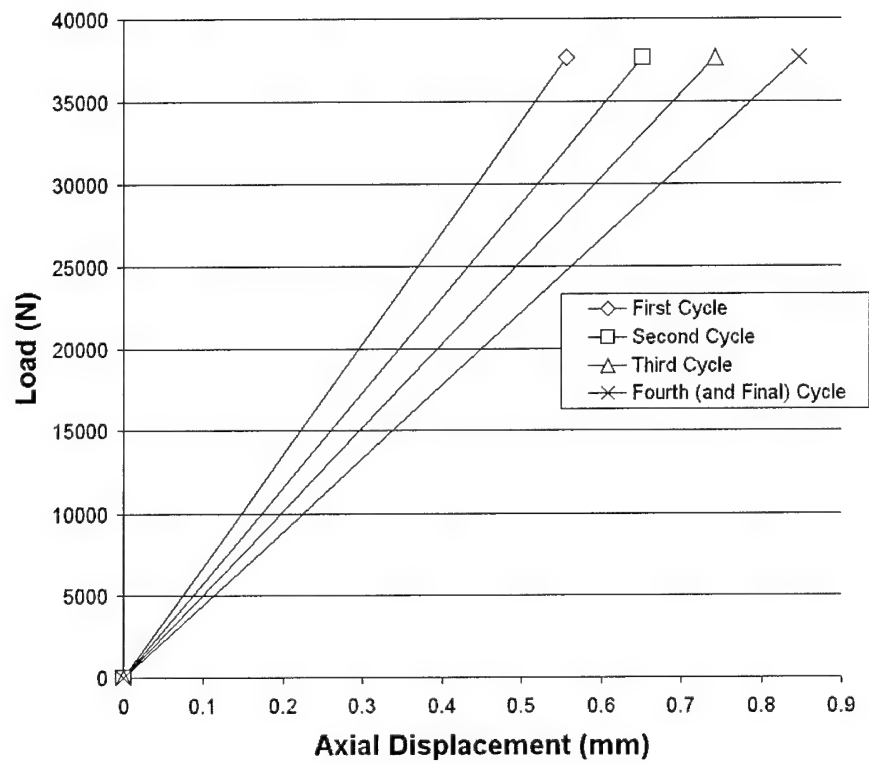
Figure 4.14   Equilibrium Curves for a Cross-Ply Panel in Fatigue with Max Strain
Criterion

V. Conclusions

This research developed a different approach to analyzing the stress of a composite shell in fatigue. This approach was built upon several proven concepts, such as the SLR theory and the Hashin failure criterion. Some key conclusions can be drawn from this research:

1. Finite Element Methods (FEM) are a useful tool to analyze composites due to their ability to determine the displacement, strain, and stress at virtually any point in the structure at any time during loading.

2. Failure criteria work well with FEM because the stresses and strains are readily available. A favorable criterion for composite laminates is the Hashin failure criterion because it analyzes multiple failure modes individually. A benefit of this criterion is the ability to tailor stiffness reduction to the type of failure that occurs, allowing a more accurate representation of the actual structure. This does not limit analysis to one type of failure mode, where other failure modes must be ignored.

3. The SLR theory, along with an algorithm for "iterating on damage" allows both material and geometric nonlinearities to be evaluated.

4. Even though the code accounts for delamination failure, delamination did not appear in any of the failure methods. If a more accurate determination of delamination is required, a theory which accounts for free-edge effects as well as stress normal to the laminate is required.

5. Fatigue causes stiffness reduction in composite materials. Stiffness reduction due to fatigue can be incorporated into existing FEM code to determine the displacement and strain in a composite cylindrical shell with a square cutout.

6. By varying the parameters R and n, it is possible to match the stiffness reduction of any composite material that displays a reduction in stiffness due to

fatigue. This also allows analysis to be tailored to any region in the fatigue life at any stress. Therefore, the given approach may be applied to a myriad of materials, geometries, and load conditions.

7. A strain-based criterion is able to determine when panel failure occurs due to a fatigue load in tension, by initiating macro-damage in the panel.

8. This technique is not limited to the first ply failure or just the initiation of damage, but is also applicable after the characteristic damage state and up to the end of the fatigue life.

Further research is necessary to validate this approach. It would also be beneficial to perform experimental analysis for comparison, as well as having a graphical post-processor to speed analysis of the results. However, this research does present a way to analyze composite materials with complex geometries under fatigue loads and determines the resulting trends. The research does not limit the type of failure to one mode, but presents more of a complete composite analysis. Not only is the initial damage determined, but fatigue effects are also incorporated as the structure is loaded.

Appendix A. SLR program guide, version fshelljb.f

The following is a description of how to compile and run the program, the appropriate cards for the input file, and a sample input file. To run the program, the FORTRAN file fshelljb.f is compiled using a SUN FORTRAN 77 compiler. In order for it to compile, open a terminal to the directory containing the fshelljb.f file. It is necessary for the compiler to read an extended line of up to 134 characters. This is done through the extend command, -e. It is also necessary for the compiler to read line continuations well into the 300's (for the stiffness arrays). The command is -Nl999 (N, l as in line, 999 for up to 999 continuation lines). The resulting input line is:

f77 -e -Nl999 fshelljb.f

Once the program compiles, the execution file is "a.out". Typing "a.out" will result in a prompt line:

WHAT IS THE INPUT FILE?

Type in the input file name. The input file should be a text file, but with no extensions. This will create two new files, with the same name but the extensions ".ans" and ".out". If the nodal forces are to be displayed, they will be displayed to the screen as it runs as well as to the .ans file. The .out file contains the input data as well as the displacements and stresses (if calculated).

The input file is made up of "cards" of data. Unless noted, if multiple entries are required for a card, separate each entry by a comma. Units are not distinguished, so it is up to the user to ensure all input properties are in compatible units. The following key is used:

- **CARD 1: title**

    The first line of the program is any text necessary to identify the file. The line may not exceed 133 characters.

- **CARD 2: iel, npe, nanal(1), nanal(2), nanal(3), imesh, nprnt, nprint, ncut**

    iel is the structure type: 1 for a plate or beam, 2 for circular cylindrical shell.

    npe is the nodes per element: either 4 or 8 (NOTE: Only an 8-noded element should be used for a cylindrical shell to maintain continuity between elements).

    nanal(1) determines the type of analysis: 0 for nonlinear analysis, 1 for linear analysis, and 2 for eigenvalue (bifurcation) analysis.

nanal(2) is for material type: 0 is an arbitrary laminate, 1 is for isotropic materials, 2 is for symmetric laminates, and 3 is for sandwich composite materials.

nanal(3) is the type of theory used: 0 for SLR (nonlinear shell theory), 1 for Von Karman plate/Donnell shell (linear theory).

imesh mesh generation: 0 for manual, 1 for automatic (always the recommended selection).

nprnt determines if the elasticity matrices are printed: 0 for no, 1 for yes. Only the initial matrices are printed.

nprint determines if the element stiffness matrices are printed: 0 for no, 1 for yes.

ncut determines the number of elements which will be removed from the mesh arrangement: enter 0 if no elements are cutout.

- **CARD 3:**

If **nanal(1)=0** (nonlinear analysis) input **intyp, ninc, imax, ires, tol, fatigue**

intyp increment type: 0 for load control, 1 for displacement control.

ninc is the number of increments of type **intyp**.

imax is the maximum number of iterations before it is assumed convergence will not be met (often on the order of 100)

ires determines how often to update the stiffness matrix: 0 for every iteration, 1 for every increment

tol tolerance to be met for convergence, often 0.1% or 0.001.

fatigue if fatigue cycles with stiffness reduction is to be used, 0 for no, 1 for yes.

If **nanal(1)=1** (linear analysis) skip this card.

If **nanal(1)=2** (eigenanalysis) read **rstep**, which is the eigenvalue step.

- **CARD 4:**

If **nanal(1)=0** (nonlinear analysis) and **fatigue=0** list **table(ninc)**, which is the table of multipliers to determine each increment step for either load or displacement control.

If **nanal(1)=0** (nonlinear analysis) and **fatigue=1** list **minval, maxval, factor**

minval is the multiplier for the minimum value in the fatigue cycle

maxval is the multiplier for the maximum value in the fatigue cycle

A-2

factor is the factor that is multiplied to reduce the stiffness terms each fatigue cycle. For example: For a 5% reduction in material properties each fatigue cycle, **factor=0.95**.

If **nanal(1)=1** (linear analysis) skip this card.

If **nanal(1)=2** (eigenanalysis) skip this card.

- **CARD 5a:**

   If **imesh=0** (manual mesh generation) read in **nem, nnm, nx, ny**

   > **nem** is the number of elements.

   > **nnm** is the number of nodes in the mesh.

   > **nx** is the number of elements in the x-direction

   > **ny** is the number of elements in the y- or s-direction

   If **imesh=1** (automatic mesh generation) just read in **nx, ny**

   > **nx** is the number of elements in the x-direction

   > **ny** is the number of elements in the y- or s-direction

- **CARD 5b:**

   If **imesh=0** (manual mesh generation) read in **nod(i), x(i), y(i)**

   > **nod(i)** is the node number

   > **x(i)** is **nod(i)'s** x position

   > **y(i)** is **nod(i)'s** y or s position.

   If **imesh=1** (automatic mesh generation) read in **dx(i)** and then **dy(i)**

   > **dx(i)** is the array of distances between the x nodes. There should be **nx** number of entries.

   > **dy(i)** is the array of distances between the y nodes. There should be **ny** number of entries.

- **CARD 6:**

   If **ncut=0** (no cutout elements) skip this card

   If **ncut='n'** ('n' number of cutout elements) read in **icut(ncut)**, which are the list of element numbers to be cutout. There should be a total of **ncut** elements listed.

- **CARD 7: LD,PO**

   > **LD** is the type of load applied: 0 for no load, 1 for transverse load, 2 for dead weight, and 3 for axial loading

   > **PO** is the stress value applied for distributed loading

- **CARD 8:** Unless **LD=3** (axial loading), skip all of **CARD 8**, including **CARD 8a and 8b**.

- **CARD 8a:** For **LD=3** (axial loading) read **nedge** which is the number of nodes with in-plane loading

- **CARD 8b:** For **LD=3** (axial loading) read **iedge(nedge)**, which is the array of nodes where in-plane loading occurs.

- **CARD 9a:** **nbdy** is the number of nodes where degrees of freedom are specified.

- **CARD 9b:** **nbound** describes which degrees of freedom at which nodes are specified. Each line of this card contains eight entries. The first entry is the node number, and the next seven entries correspond to the degrees of freedom $[u, v, w, w_{,x}, w_{,s}, \Psi_x, \Psi_y]$. If the degree of freedom is not specified, a zero is placed in its space. If it is to be specified, a one is placed in its corresponding position. For example, if degrees of freedom u, v, and w are to be specified for node 112 and degrees of freedom $w_{,x}$ and $w_{,s}$ are to be specified for node 114, the entries would appear:

  112,1,1,1,0,0,0,0
  114,0,0,0,1,1,0,0

  There should be **nbdy** number of lines to this card. A carriage return is necessary between node entries, but a comma is not.

- **CARD 9c:** **vbdy(i)** is an array of the prescribed displacements from above. They are sequentially placed. From the example above, **vbdy(i)** would contain five entries.

- **CARD 10:** **nbsf** is the number of degrees of freedom containing arbitrary loads.

- **CARD 10a:** **ibsf(i)** is an array of **nbsf** node numbers with prescribed loads. This card is skipped if **nbsf** is zero.

- **CARD 10b:** **vbsf(i)** is an array of the loads corresponding to the degrees of freedom in **ibsf(i)**, therefore sequence is important. Again, this card is skipped if **nbsf** is zero.

- **CARD 11:** is for the material properties.

  If **nanal(2)=1** (isotropic), enter **ey, pnu, ht**.

  > **ey** is Young's modulus.

  > **pnu** is Poisson's ratio.

  > **ht** is the thickness.

  If **nanal(2)=0,2** (composite laminate), enter **e1,e2,g12,pnu12,g13,g23**

  > **e1** is the modulus in the 1 or fiber direction.

A-4

e2 is the 2 or matrix modulus.

g12 is the shear modulus in the 1-2 direction.

pnu12 is the Poisson's ratio in the 1-2 direction

g13, g23 are the shear moduli in the 1-3 and 2-3 directions, respectively.

If **nanal(2)=3** (sandwich) then the material is a sandwich composite and the same variables entered for **nanal(2)=0,2** are entered for the sandwich facesheets only.

- **CARD 11a: e1s, e2s, g12s, pnu12s,g13s, g12s** This card is used only when **nanal(2)=3**. The above properties have the same definition, except they apply to the sandwich core material.

- **CARD 11b:** If **nanal(2)=1**, (isotropic) skip this card.

  If **nanal(2)=0,2** (composite), read in **np, pt**

    np is the number of plies.

    pt is the average ply thickness.

  If **nanal(2)=3** (sandwich composite), read in **np, pt, pts**

    np is the number of layers in the facesheets,

    pt is the thickness of the facesheet

    pts is the thickness of the core.

- **CARD 11c:**

  If **nanal(2)=1** (isotropic), skip this card.

  If **nanal(2)=0,2,3** (composites), read in **the(i)** which is the orientation of the plies (in degrees) within the laminate. For the sandwich material, it is the orientation of the facesheet plies.

- **CARD 12:** If **iel=1** (flat plate), skip this card.

  Otherwise, read in **rad**, which is the cylinder shell radius.

- **CARD 13: nfor** is the number of degrees of freedom where the nodal forces are to output.

- **CARD 13a: ifor(nfor)** is an array of **nfor** global degree of freedom numbers where the nodal forces will be calculated and output. For example, in displacement control, it might be beneficial to know the resulting forces along the edge where the displacements are input.

- **CARD 14a: nstress, ifail, icrit**

    nstress is the number of elements where stress calculations are to take place. If failure criteria are used, this number will be automatically (internally) set to the number of elements.

A-5

ifail determines if failure analysis is used: 0 for no failure analysis, 1 for failure analysis.

icrit when **ifail=1**, this variable determines the type of criterion used: 1 for Hashin, 2 for Lee, 3 for Maximum stress.

- **CARD 14b:**

  If **ifail=1** (failure analysis) and **nanal(2)=0,2,3** (composite laminate) read in **sigfn, sigfs, sigmt, sigmc, sigms, sigdt, sigds** corresponding to the material strengths of the chosen composite. The fourth letter corresponds to: f for fiber, m for matrix, and d for delamination. The fifth letter represents: n for normal, s for shear, t for tension, c for compression.

- **CARD 14c:**

  If **nanal(2)=3** (sandwich) also enter the core material strengths for failure evaluation. The required strengths are **sigcr, sig13c, sig23c**

  sigcr is the transverse direct strength.

  sig13c is the transverse core shear strength in the 1-2 direction.

  sig23c is the core shear strength in the 1-3 direction.

1/4 of 24 x 24, [0/90]2s, Tension, Load Control, Use Failure
2,8,0,2,0,1,0,0,16
0,11,80,0,0.001,1
0.1,1.0,0.88
12,12
0.25,0.25,0.25,0.25,0.25,0.25,0.25,0.25,
0.25,0.25,0.25,0.25,0.25,0.25,0.25,0.25,
0.25,0.25,0.25,0.25,0.25,0.25,0.25,0.25,
0.25,0.25,0.25,0.25,0.25,0.25,0.25,0.25,
0.25,0.25,0.25,0.25,0.25,0.25,0.25,0.25,
0.25,0.25,0.25,0.25,0.25,0.25,0.25,0.25
105,106,107,108,117,118,119,120,
129,130,131,132,141,142,143,144
3,-17146.
25
1,26,39,64,77,102,115,140,153,178,
191,216,229,254,267,292,305,330,343,
368,381,406,419,444,457
106
25,1,0,0,1,0,1,0
38,1,0,0,0,0,0,0
63,1,0,0,1,0,1,0
76,1,0,0,0,0,0,0
101,1,0,0,1,0,1,0
114,1,0,0,0,0,0,0
139,1,0,0,1,0,1,0
152,1,0,0,0,0,0,0
177,1,0,0,1,0,1,0
190,1,0,0,0,0,0,0
215,1,0,0,1,0,1,0
228,1,0,0,0,0,0,0
253,1,0,0,1,0,1,0
266,1,0,0,0,0,0,0
291,1,0,0,1,0,1,0
304,1,0,0,0,0,0,0
329,1,0,0,1,0,1,0
342,1,1,0,0,0,0,0
367,1,1,1,1,1,1,1
380,1,1,0,0,0,0,0
405,1,1,1,1,1,1,1
418,1,1,0,0,0,0,0
443,1,1,1,1,1,1,1

456,1,1,0,0,0,0,0
481,1,1,1,1,1,1,1
458,0,1,0,0,0,0,0
459,0,1,0,0,1,0,1
460,0,1,0,0,0,0,0
461,0,1,0,0,1,0,1
462,0,1,0,0,0,0,0
463,0,1,0,0,1,0,1
464,0,1,0,0,0,0,0
465,0,1,0,0,1,0,1
466,0,1,0,0,0,0,0
467,0,1,0,0,1,0,1
468,0,1,0,0,0,0,0
469,0,1,0,0,1,0,1
470,0,1,0,0,0,0,0
471,0,1,0,0,1,0,1
472,0,1,0,0,0,0,0
473,0,1,0,0,1,0,1
1,0,1,1,1,1,1,1
26,0,1,0,0,0,0,0
39,0,1,1,1,1,1,1
64,0,1,0,0,0,0,0
77,0,1,1,1,1,1,1
102,0,1,0,0,0,0,0
115,0,1,1,1,1,1,1
140,0,1,0,0,0,0,0
153,0,1,1,1,1,1,1
178,0,1,0,0,0,0,0
191,0,1,1,1,1,1,1
216,0,1,0,0,0,0,0
229,0,1,1,1,1,1,1
254,0,1,0,0,0,0,0
267,0,1,1,1,1,1,1
292,0,1,0,0,0,0,0
305,0,1,1,1,1,1,1
330,0,1,0,0,0,0,0
343,0,1,1,1,1,1,1
368,0,1,0,0,0,0,0
381,0,1,1,1,1,1,1
406,0,1,0,0,0,0,0
419,0,1,1,1,1,1,1
444,0,1,0,0,0,0,0

457,0,1,1,1,1,1,1
339,1,1,0,0,0,0,0
340,1,1,0,0,0,0,0
341,1,1,0,0,0,0,0
360,1,1,0,0,0,0,0
361,1,1,1,1,1,1,1
362,1,1,0,0,0,0,0
363,1,1,1,1,1,1,1
364,1,1,0,0,0,0,0
365,1,1,1,1,1,1,1
366,1,1,0,0,0,0,0
377,1,1,0,0,0,0,0
378,1,1,0,0,0,0,0
379,1,1,0,0,0,0,0
398,1,1,0,0,0,0,0
399,1,1,1,1,1,1,1
400,1,1,0,0,0,0,0
401,1,1,1,1,1,1,1
402,1,1,0,0,0,0,0
403,1,1,1,1,1,1,1
404,1,1,0,0,0,0,0
415,1,1,0,0,0,0,0
416,1,1,0,0,0,0,0
417,1,1,0,0,0,0,0
436,1,1,0,0,0,0,0
437,1,1,1,1,1,1,1
438,1,1,0,0,0,0,0
439,1,1,1,1,1,1,1
440,1,1,0,0,0,0,0
441,1,1,1,1,1,1,1
442,1,1,0,0,0,0,0
453,1,1,0,0,0,0,0
454,1,1,0,0,0,0,0
455,1,1,0,0,0,0,0
474,1,1,0,0,0,0,0
475,1,1,1,1,1,1,1
476,1,1,0,0,0,0,0
477,1,1,1,1,1,1,1
478,1,1,0,0,0,0,0
479,1,1,1,1,1,1,1
480,1,1,0,0,0,0,0
0.,0.,0.,0.,0.,0.,0.,0.,0.,0.,

0.,0.,0.,0.,0.,0.,0.,0.,0.,0.,
0.,0.,0.,0.,0.,0.,0.,0.,0.,0.,
0.,0.,0.,0.,0.,0.,0.,0.,0.,0.,
0.,0.,0.,0.,0.,0.,0.,0.,0.,0.,
0.,0.,0.,0.,0.,0.,0.,0.,0.,0.,
0.,0.,0.,0.,0.,0.,0.,0.,0.,0.,
0.,0.,0.,0.,0.,0.,0.,0.,0.,0.,
0.,0.,0.,0.,0.,0.,0.,0.,0.,0.,
0.,0.,0.,0.,0.,0.,0.,0.,0.,0.,
0.,0.,0.,
0.,0.,0.,0.,0.,0.,0.,
0.,0.,0.,0.,0.,0.,0.,
0.,0.,0.,0.,0.,0.,0.,
0.,0.,0.,0.,0.,0.,0.,
0.,0.,0.,0.,0.,0.,0.,
0.,0.,0.,0.,0.,0.,0.,
0.,0.,0.,0.,0.,0.,0.,
0.,0.,0.,0.,0.,0.,0.,
0.,0.,0.,0.,0.,0.,0.,
0.,0.,0.,0.,0.,0.,0.,
0.,0.,0.,0.,0.,0.,0.,
0.,0.,0.,0.,0.,0.,0.,
0.,0.,0.,0.,0.,0.,
0.,0.,0.,0.,0.,0.,0.,0.,0.,0.,
0.,0.,0.,0.,0.,0.,0.,0.,0.,0.,
0.,0.,0.,0.,0.,0.,0.,0.,0.,0.,
0.,0.,0.,0.,0.,0.,0.,0.,0.,0.,
0.,0.,0.,0.,0.,0.,0.,0.,0.,0.,
0.,0.,0.,0.,0.,0.,0.,0.,0.,0.,
0.,0.,0.,0.,0.,0.,0.,0.,0.,0.,
0.,0.,0.,0.,0.,0.,0.,0.,0.,0.,
0.,0.,0.,0.,0.,0.,0.,0.,0.,0.,
0.,0.,0.,0.,0.,0.,0.,0.,0.,0.,
0.,0.,0.,0.,0.,0.,0.,0.,0.,0.,
0.,0.,0.,0.,0.,0.,0.,0.,0.,0.,
0.,0.,0.,0.,0.,0.,0.,0.,0.,0.,
0.,0.,0.,0.,0.,0.,0.,0.,0.,0. 0
19.7e6,1.579e6,0.925e6,0.276,0.925e6,0.462e6
8,0.00514
0.,90.,0.,90.,90.,0.,90.,0.
12.0
25

1,116,142,257,283,398,424,
539,565,680,706,821,847,
962,988,1103,1129,1244,1270,
1385,1411,1526,1552,1667,1693
0,1,1
216.1e3,31.7e3,6.31e3,6.31e3,6.31e3,7.20e3,12.39e3,17.39e3

Bibliography

1. A. S. Saada. *Elasticity, Theory and Applications*. Krieger Publishing Company, Malabar, Florida, USA, second edition, 1993.

2. L. H. Donnell. Stability of thin walled tubes under torsion. Technical Report NACA 479, NACA, 1933.

3. E. Reissner. The effects of transverse shear deformation on the bending of elastic plates. *Journal of Applied Mechanics*, 12:A69–A77, 1945.

4. R. D. Mindlin. Influence of rotatory inertia and shear on flexural motion of isotropic elastic plates. *Journal of Applied Mechanics*, 18:31–38, 1951.

5. A. N. Palazotto and S. T. Dennis. *Nonlinear Analysis of Shell Structures*. AIAA, Washington, DC, 1992.

6. J. C. Hatfield. Effects of thickness and ply layup on the collapse characteristics of cylindrical composite shells with large cutouts. Master's thesis, Air Force Institute of Technology, 1992.

7. E. Senocak and A. M. Waas. Optimally reinforced cutouts in laminated circular cylindrical shells. *Journal of Mechanical Sciences*, 38(2):121–140, 1996.

8. M. W. Hilburger, A. M. Waas, and J. H. Starnes Jr. Response of composite shells with cutouts to internal pressure and compression loads. *AIAA Journal*, 37(2):232–237, Feb. 1999.

9. R. K. Kapania, S. G. Haryadi, and R. T. Haftka. Global/local analysis of commposite plates with cutouts. *Computational Mechanics*, 19:386–396, 1997.

10. J. Rhee, S. He, and R. E. Rowlands. Hybrid moiré-numerical stress analysis around cutouts in loaded composites. *Experimental Mechanics*, 36(4):379–387, Dec 1996.

11. T. D. Gerhardt. A hybrid/finite element approach for stress analysis of notched anisotropic materials. *Journal of Applied Mechanics*, 51:804–810, Dec. 1984.

12. H. Chao, L. Diankui, M. Xingrui, and W. Benli. On the stress concentration in thick cylindrical shells with an arbitrary cutout. *Applied Mathematics and Mechanics*, 19(5):399–410, May 1998.

13. S. W. Tsai. Strength characteristics of composite materials. Technical Report NASA-CR-224, NASA, 1965.

14. R. Hill. A theory of the yielding and plastic flow of anisotropic materials. In *Proceedings of the Royal Society*, volume 193 of *A*, 1948.

15. S. W. Tsai and E. M. Wu. A general theory of strength for anisotropic materials. *Journal of Composite Materials*, 5:58, 1971.

16. Z. Hashin. Failure criteria for unidirectional fiber composites. *Journal Of Applied Mechanics*, 47:329–334, June 1980.

17. O. Hoffman. The brittle strength of orthotropic materials. *Journal of Composite Materials*, 1:200, 1967.

18. J. D. Lee. Three dimensional finite element analysis of damage accumulation in composite laminate. *Computers and Structures*, 15(3):335–350, 1982.

19. B. G. Falzon, G. P. Steven, and Y. M. Xie. Shape optimization of interior cutouts in composite panels. *Structural Optimization*, 11:43–49, 1996.

20. M. S. Spottswood. Progressive failure analysis of composite panels. Master's thesis, Air Force Institute of Technology, 1999.

21. D. Broek. *Elementary Engineering Fracture Mechanics*. Kluwer Academic Publishers, Boston, fourth edition, 1986.

22. B. D. Agarwal and L. J. Broutman. *Analysis and Performance of Fiber Matrix Composites*. John Wiley and Sons, INC., New York, second edition, 1990.

23. K. L. Reifsnider, E. G. Henneke II, and W. W. Stinchcomb. Technical Report AFML-TR-76-81, USAF, 1979.

24. R. Talareja. *Fatigue of Composite Materials*. Technomic Publishing Co., London, 1987.

25. K. Ericson, M. Persson, L. Carlsson, and A. Gustavsson. On the prediction of the initiation of delamination in a $[0/90]_s$ laminate with a circular hole. *Journal of Composite Materials*, 18:495–506, 1984.

26. K. C. Jen and C. T. Sun. Matrix cracking and delamination prediction in graphite/epoxy laminates. *Journal of Reinforced Plastics and Composites*, 11:1163–1175, 1992.

27. G. P. Sendeckyj. Life prediction for resin-matrix composite materials. In Reifsnider (28), pages 431–480.

28. K. L. Reifsnider, editor. *Damage and Damage Mechanics*, volume 4 of *Composite Materials Series*, New York, 1991. Elsevier.

29. J. R. Schaff and B. D. Davidson. A strength-based wearout model for predicting the life of composite structures. In E. A. Armanos, editor, *Composite Materials: Fatigue and Fracture, ASTM STP 1285*, volume 6, 1997.

30. W. W. Stinchcomb and C. E. Bakis. Fatigue behavior of composite laminates. In Reifsnider (28), pages 105–178.

31. R. D. Jamison and K. L. Reifsnider. Technical Report AFWAL-TR-82-3103, USAF, 1982.

32. A. Poursartip, M. F. Ashby, and P. W. R. Beaumont. The fatigue damage mechanics of a carbon fibre composite laminate: Ii-life prediction. *Composites Science and Technology*, 25:283–298, 1986.

33. T. K. O'Brien. Characterization of delamination onset and growth in a composite laminate. In K. L. Reifsnider, editor, *Damage in Composite Materials, ASTM STP 775*, 1982.

34. M.-H. R. Jen, Y. S. Kau, and J. M. Hsu. Initiation and propagation of delamination in a centrally notched composite laminate. *Journal of Composite Materials*, 27:272–302, 1993.

35. R. Barboni, R. Carbonaro, and P. Gaudenzi. The effects of delamination on the fatigue behavior of composite structures. *Journal of Composite Materials*, 33(3):267–303, 1999.

36. Z. Hashin and A. Rotem. A fatigue criterion for fiber reinforced materials. *Journal of Composite Materials*, 7:448–464, 1973.

37. Z. Fawaz and F. Ellyin. Fatigue failure model for fibre-reinforced materials under general loading conditions. *Journal of Composite Materials*, 28(15):1432–1451, 1994.

38. T. P. Philippidis and A. P. Vassilopoulos. Fatigue strength prediction under multiaxial stress. *Journal of Composite Materials*, 33(17):1578–1599, 1999.

39. V. L. Tahiri, C. Hénaff-Gardin, and M. C. Lafarie-Frenot. Damage in in-plane shear behaviour of a ($\pm45°$) carbon/epoxy laminate under quasi-static and fatigue tensile loadings. In G. Lütjering and H. Nowack, editors, *Fatigue '96, Proceedings of the Sixth International Fatigue Congress*, volume 3, 1996.

40. F. B. Hildebrand, E. Reissner, and G. B. Thomas. Notes on the foundation of the theory of small displacements of orthotropic shells. Technical Report NACA-TN-1833, NACA, 1949.

41. R. D. Cook, D. S. Malkus, and M. E. Plesha. *Concepts and Applications of Finite Element Analysis*. John Wiley and Sons, New York, third edition, 1989.

42. I. M. Daniel and O. Ishai. *Engineering Mechanics of Composite Materials*. Oxford University Press, New York, 1994.

43. R. S. Sandhu. Nonlinear behavior of unidirectional and angle ply laminates. *Journal of Aircraft*, 13(1):104–111, Feb. 1976.

44. S. W. Tsai. A survey of macroscopic failure criteria for composite materials. *Journal of Reinforced Plastics and Composites*, 13:40–62, January 1984.

45. A. Poursartip, M. F. Ashby, and P. W. R. Beaumont. The fatigue damage mechanics of a carbon fibre composite laminate: I-development of the model. *Composites Science and Technology*, 25:193–218, 1986.

46. S. T. Dennis. *Large Displacement and Rotation Formulation for Laminated Cylindrical Shells Including Parabolic Transverse Shear*. PhD thesis, Air Force Institute of Technology, 1988.

47. J. A. Daniels, A. N. Palazotto, and R. S. Sandhu. Failure characteristics iin thermoplastic composite laminates due to an eccentric circular discontinuity. *AIAA Journal*, 29(5):830–837, May 1991.

Vita

Joshua Todd Boatwright was born in Tupelo, Mississippi on 18 April 1973. He graduated from Pontotoc High School, Pontotoc, Mississippi on 31 May 1991. Four years later, on 31 May 1995, he graduated from the United States Air Force Academy, Colorado Springs, CO, and was commissioned a Second Lieutenant in the United States Air Force. His first assignment was as an aeronautical engineer in the Structures Branch of the C-5 Aircraft Directorate, San Antonio Air Logistics Center, Kelly AFB, San Antonio, TX. Engineering tasks in the C-5 Aircraft Directorate included ensuring structural integrity for the C-5 fleet, such as developing repairs for structural damage which exceeded conventional repair limits and instituting fleet-wide modifications. He also served as a technical evaluator on the contract proposal review team for the C-5 Depot Maintenance Public-Private Competition and was a qualified Aircraft Battle Damage Repair (ABDR) Engineer. In August 1998, he was assigned to the Air Force Institute of Technology (AFIT) to pursue a Master's Degree in Aeronautical Engineering. Upon completion of the AFIT program, he will be assigned to the Air Vehicles Directorate, Air Force Research Labs, Wright-Patterson AFB, Dayton, Ohio. He is a member of the Sigma Gamma Tau aeronautical engineering honor society, the American Institute of Aeronautics and Astronautics, is a registered Engineering Intern in the state of Ohio, and is listed in *Who's Who in America, Science and Engineering, 5th edition.*

Joshua married Kammie J. Moberly of Denver, Colorado on 13 April 1996. He is the son of the late William R. and Margarette L. Boatwright.

Permanent address: 2921 Revere Ave.
                       Dayton, OH 45420-1725

REPORT DOCUMENTATION PAGE

Form Approved
OMB No. 0704-0188

1. AGENCY USE ONLY *(Leave blank)*	2. REPORT DATE	3. REPORT TYPE AND DATES COVERED
	March 2000	Masters Thesis

4. TITLE AND SUBTITLE
FINITE ELEMENT ANALYSIS OF A COMPOSITE CYLINDRICAL SHELL WITH A CUTOUT UNDER A FATIGUE LOAD

5. FUNDING NUMBERS

6. AUTHOR(S)
Joshua T. Boatwright, Captain, USAF

7. PERFORMING ORGANIZATION NAME(S) AND ADDRESS(ES)
Air Force Institute of Technology
Department of Aeronautical and Astronautical Engineering
2950 P. Street, Bldg 640
WPAFB, OH 45433

8. PERFORMING ORGANIZATION REPORT NUMBER

AFIT/GAE/ENY/00M-03

9. SPONSORING/MONITORING AGENCY NAME(S) AND ADDRESS(ES)
Dr. Stephen Walker
Air Force Office of Scientific Research
AFOSR/NA
801 North Randolph Street, Room 732
Arlington, VA 22203-1997 ph. (703)696-6962

10. SPONSORING/MONITORING AGENCY REPORT NUMBER

11. SUPPLEMENTARY NOTES
Advisor: Anthony N. Palazotto, PhD.
2950 P. Street, Bldg 640
WPAFB, OH 45433 ph. (937) 255-3636 ext. 4599 Anthony.Palazotto@afit.af.mil

12a. DISTRIBUTION AVAILABILITY STATEMENT
Distribution Unlimited

12b. DISTRIBUTION CODE

13. ABSTRACT *(Maximum 200 words)*
A higher-order shell theory is used to analyze compressive and tensile loads on a graphite/epoxy laminated cylinder containing a square cutout. The Hashin failure criterion is used to determine failure in the fiber, matrix, or lamination. Once failure occurs, the appropriate stiffness terms are reduced. This failure causes a redistribution of stress, leading to further failure. In order to account for the loss of residual strength due to cyclic loading, the stiffness matrix is further reduced at each new increment of load or displacement. The objective is not to determine the S-N curve for the material, but rather to determine the damage, displacement, and stress distribution in a complex configuration under fatigue loading using a progressive failure and stiffness reduction approach. The failure progression for static loads is determined and used as an indicator for the cyclic loads. In fatigue, it is shown that as the stiffness decreases, the global displacements and strains increase. The maximum strain failure criterion is then used, and eventually the entire panel fails.

14. SUBJECT TERMS
composite, cylinder, shell, cutout, failure, fatigue

15. NUMBER OF PAGES
110

16. PRICE CODE
N/A

17. SECURITY CLASSIFICATION OF REPORT	18. SECURITY CLASSIFICATION OF THIS PAGE	19. SECURITY CLASSIFICATION OF ABSTRACT	20. LIMITATION OF ABSTRACT
UNCLASSIFIED	UNCLASSIFIED	UNCLASSIFIED	UL